arXiv:1304.5521v1 [math.AP] 26 Mar 2013

Vortex Filament Equation for a Regular Polygon

F. de la Hoz[a,*], L. Vega[b]

[a]Department of Mathematics, Statistics and Operations Research, Faculty of Science and Technology, University of the Basque Country UPV/EHU, Barrio Sarriena S/N, 48940 Leioa, Spain
[b]Department of Mathematics, Faculty of Science and Technology, University of the Basque Country UPV/EHU, Barrio Sarriena S/N, 48940 Leioa, Spain

---

Abstract

In this paper, we study the evolution of the localized induction approximation (LIA), also known as vortex filament equation,

$$\mathbf{X}_t = \mathbf{X}_s \wedge \mathbf{X}_{ss},$$

for $\mathbf{X}(s,0)$ a regular planar polygon. Using algebraic techniques, supported by full numerical simulations, we give strong evidence that $\mathbf{X}(s,t)$ is also a polygon at any rational time; moreover, it can be fully characterized, up to a rigid movement, by a generalized quadratic Gauß sum.

We also study the fractal behavior of $\mathbf{X}(0,t)$, relating it with the so-called Riemann's non-differentiable function, that, as proved by S. Jaffard, fits with the multifractal model of U. Frisch and G. Parisi, for fully developed turbulence.

Keywords:
vortex filament equation, Schrödinger map, generalized quadratic Gauß sums, pseudo-spectral methods, fractals

---

1. Introduction

Given a curve $\mathbf{X}_0 : \mathbb{R} \longrightarrow \mathbb{R}^3$, we consider the geometric flow

$$\mathbf{X}_t = c\,\mathbf{b}, \tag{1}$$

---

[*] Corresponding author

Email addresses: `francisco.delahoz@ehu.es` (F. de la Hoz), `luis.vega@ehu.es` (L. Vega) where c is the curvature and $\mathbf{b}$ the binormal component of the Frenet-Serret formulae

$$\begin{pmatrix} \mathbf{T} \\ \mathbf{n} \\ \mathbf{b} \end{pmatrix}_s = \begin{pmatrix} 0 & c & 0 \\ -c & 0 & \tau \\ 0 & -\tau & 0 \end{pmatrix} \cdot \begin{pmatrix} \mathbf{T} \\ \mathbf{n} \\ \mathbf{b} \end{pmatrix}. \tag{2}$$

The flow can be expressed as as

$$\mathbf{X}_t = \mathbf{X}_s \wedge \mathbf{X}_{ss}, \tag{3}$$

where $\wedge$ is the usual cross-product, t is the time, and s is the arc-length parameter. It appeared for the first time in 1906 [1] and was rederived in 1965 by Arms and Hama [2] as an approximation of the dynamics of a vortex filament under the Euler equations. This model is usually known as the localized induction approximation (LIA); we refer the reader to [3] and [4] for an analysis and discussion of its limitations.

(1) and (3) are also known as the binormal equation and the vortex filament equation, respectively. Some of their explicit solutions are the line, the circle, and the helix. Since the tangent vector $\mathbf{T} = \mathbf{X}_s$ remains with constant length, we can assume that $\mathbf{T} \in \mathbb{S}^2$, $\forall t$. Differentiating (3), we get the so-called Schrödinger map equation on the sphere:

$$\mathbf{T}_t = \mathbf{T} \wedge \mathbf{T}_{ss}, \tag{4}$$

which is a particular case of the Landau-Lifshitz equation for ferromagnetism [5]. (4) can be rewritten in a more geometric way as

$$\mathbf{T}_t = \mathbf{J}\mathbf{D}_s\mathbf{T}_\mathbf{s}, \tag{5}$$

where $\mathbf{D}$ is the covariant derivative, and $\mathbf{J}$ is the complex structure of the sphere. Written in this way, (4) can be generalized to more general definition domains and images, as the hyperbolic plane $\mathbb{H}^2$.

(3) is time reversible, i.e., if $\mathbf{X}(s, t)$ is a solution, so is $\mathbf{X}(-s, -t)$. Bearing in mind this fact, an important property of (3) (and, hence, of (4)) is that it has a one-parameter family of regular self-similar solutions that develop a corner-shaped singularity at finite time. This was proved in [6] for the Euclidean case, and in [7], for the hyperbolic case. Furthermore, starting from T. F. Buttke's work [8], there have been a couple of papers devoted to studying numerically the self-similar solutions of (3), as in [9], where a careful numerical study of those solutions for both the Euclidean and the hyperbolic

cases was done. In [9], on the one hand, the authors reproduced numerically the formation of the corner-shaped singularity, and, on the other hand, they started with a corner-shaped initial datum, recovering numerically the self-similar solutions; in all cases, the correct choice of boundary conditions was shown to be vital. Furthermore, they gave numerical evidence that fractality phenomena appeared in (4), if, for instance, fixed boundary conditions were imposed on $\mathbf{T}$. Remark that the relationship between fractals and the Schrödinger map is not new; indeed, in [10], an aortic valve model was proposed, in order to study the apparent fractal character of the valve's fiber architecture. Instead of $\mathbf{X}(s,t)$, the authors wrote $\mathbf{X}(u,v)$, where v, which corresponds to our time, is such that the curves $v =$ constant are the fibers. After imposing fixed boundary conditions at $u = \pm u_0$, they showed that the curves $u =$ constant have a fractal character. Besides, the fractal dimension of those curves was calculated numerically in [11].

Even if the solutions of (3) for an initial datum with a corner are well understood, nothing had been done for more general initial data with several corners, in particular, polygons. Nevertheless, in a recent submitted paper [12] by R. Jerrard and D. Smets, they propose a global existence theorem that allows to consider such types of initial data. Moreover, they simulate numerically the evolution of the unit square at different times, suggesting that the solution could become again polygonal; indeed, at a certain time, the square seems to reappear, but rotated $\pi/4$ with respect to the initial one. In the following pages, we will show not only that these observations are correct, but that, given a regular planar polygon as initial datum, we have a completely describable polygon at any rational time.

The structure of this paper is as follows. In Section 2, we apply the Hasimoto transformation to (4), but considering a variation of the Frenet-Serret formulae (2). This relates (3) and (4) with the nonlinear Schrödinger (NLS) equation:

$$\psi_t = i\psi_{ss} + i\left(\frac{1}{2}(|\psi|^2 + A(t))\right)\psi, \quad A(t) \in \mathbb{R}, \tag{6}$$

where $A(t) \in \mathbb{R}$ can be written in terms of $c(0,t)$, $\tau(0,t)$ and their derivatives. The fact that (3)-(4) and the NLS equation are related has far-reaching consequences.

In Section 3, we gather all the theoretical arguments that support our numerical experiments. We start recalling some elemental geometric symmetries that regular polygons have and that are preserved by LIA. On the one hand, these symmetries greatly simplify the numerical implementation and, on the other hand, they play a fundamental role in computing some important quantities that govern the dynamics of regular polygons. Then, we pay special attention to a group of symmetries that, as far as we know, can only be visualized through the use of the Hasimoto transformation and the NLS equation (6). These are the so-called Galilean transformations (33), that leave invariant the set of solutions of LIA.

We will proceed as in [13], where the solution of NLS that has the delta function as an initial condition is characterized by the fact that it leaves invariant all the Galilean transformations. This property determines the solution, except for one function of time that is easily computed by solving a simple ODE and choosing $A(t)$ in (6) appropriately. This argument heavily relies on assuming that uniqueness holds for such a singular initial datum. This is in indeed a quite delicate question that in the case of just one delta (i.e. a curve with just one corner) has needed some work to be eventually answered in the positive [14, 15, 16]. However, in this paper, we are interested in just proving the existence of a solution starting with a polygon. Therefore, we can assume uniqueness to conclude that the expected solution has as many symmetries as possible and simplify in this way the analysis.

In our case, we take a planar regular polygon of M sides as initial datum. In terms of NLS, this amounts to considering periodic boundary conditions and an initial datum which is given by an infinite sum of delta functions with appropriate weights. Therefore, just a subgroup of the group of the Galilean transformations has to be considered. Then, as in [13], the solution of (6) is determined except, again, for a function that will depend on time. But, in this case, it is very delicate how to determine this function and does not seem to be easy. Moreover, a very simple analysis makes clear that it cannot be expected to make any sense to the NLS equation (6). In fact, the arguments in [16] prove that, in the case of an initial condition given by a curve with just one corner, (6) does not make sense in an interval of time that contains $t = 0$. Our approach in this paper is to integrate the Frenet-Serret system (18) with $\psi(s,t) = \alpha + i\beta$ the distribution given by

$$\psi(s,t) = \hat{\psi}(0,t) \sum_{k=-\infty}^{\infty} e^{-i(Mk)^2 t + iMks}. \tag{7}$$

We do it just for times that are rational multiples of $2\pi/M^2$, that is to say, of the form $t_{pq} = (2\pi/M^2)(p/q)$, because in that case the corresponding curve is a skew polygon with Mq sides, for q odd, and with $Mq/2$ sides, for q even, determined by a generalized quadratic Gauss sum:

$$G(a,b,c)=\sum_{l=0}^{c-1}e^{2\pi i(al^2+bl)/c},\quad a,b\in\mathbb{Z},c\in\mathbb{Z}-\{0\}. \tag{8}$$

The function of time $\hat{\psi}(0,t)$ is then obtained by imposing the condition that the polygon has to be closed. As a consequence, the tangent vector is fixed, except for a rotation that can depend on time. This rotation is determined by using the extra symmetries that are available for regular polygons and that we have already mentioned. The next step is to integrate $\mathbf{T}$, in order to obtain $\mathbf{X}$ at rational times. Using again the symmetries, we are able to calculate all the necessary quantities, except for some possible translation in the z direction that can be easily computed numerically. Nevertheless, we do not see a simple way of obtaining this last value using just theoretical arguments.

At this point it is important to recall the invariances of the so-called Jacobi theta function, which is closely related to (7):

$$\theta(s,t)=\sum_{k=-\infty}^{\infty}e^{-\pi ik^2t+2\pi iks}. \tag{9}$$

This function is precisely the solution of the linear Schrödinger equation

$$\psi_t=\frac{i}{4\pi}\psi_{ss}, \tag{10}$$

with a 1-periodic delta as the initial condition. Therefore the Galilean transformations still hold in this case; moreover, they also imply the extra symmetry

$$\theta(s,t)=e^{i\pi/4}\frac{e^{\frac{\pi is^2}{t}}}{\sqrt{t}}\theta\left(\frac{s}{t},\frac{-1}{t}\right),\quad t>0, \tag{11}$$

which, together with the periodicity property,

$$\theta(s,t+2)=\theta(s,t), \tag{12}$$

generates the so-called unimodular subgroup. In fact, in [17, 18], all these symmetries are used to prove the existence of a continuum range of exponents (usually known as the spectrum of singularities) for the Hölder regularity of

$$\phi(t)=\sum_{k=1}^{\infty}\frac{e^{\pi i k^2 t}}{i\pi k^2},\quad t\in[0,2], \tag{13}$$

whose real part is precisely Riemann's non-differentiable function:

$$f(t)=\sum_{k=1}^{\infty}\frac{\sin(\pi k^2 t)}{\pi k^2}. \tag{14}$$

More concretely, in [18] it is proved that Riemann's non-differentiable function is a multifractal. In other words, it is proved that the set of times t that have the same Hölder exponent is a fractal with a dimension depending on the Hölder exponent, in such a way that the conjecture stated by U. Frisch and G. Parisi in [19] is fulfilled (see also [20], for more details at this respect and the connection of this question with fully developed turbulence and intermittency).

From all this, it is very natural to ask if something similar happens with the evolution of a regular polygon by LIA. There are different ways of understanding the question. One is whether, for a fixed time, the corresponding curve is a fractal or even a multifractal. From what we have said above, this cannot happen for rational times, because, in this case, it is a skew polygon. But precisely these examples do suggest that quite likely the situation for irrational times is completely different; and in fact it is, as it is explained in Section 5.2. At this respect, we have to call the attention of [21], where upper bounds for the regularity of (9) measured in Besov spaces of negative indices are obtained.

On the other hand, we could also ask if something similar to the properties of Riemann's non-differentiable function also holds in our case. It is very easy to find the analogous to (13) in out setting. In fact, for a given M, if we write $\mathbf{X}(0,t)=(X_1(0,t),X_2(0,t),X_3(0,t))$, bearing in mind the symmetries of the problem, we conclude that $\mathbf{X}(0,t)$ is a planar curve, so we identify the plane where it lives with $\mathbb{C}$ and define

$$z(t)=-\|(X_1(0,t),X_2(0,t))\|+iX_3(0,t). \tag{15}$$

This curve, or, more precisely, $z(t)-c_Mt$, for a certain $c_M>0$ that depends on M, can be seen as nonlinear versions of (13). Is $z(t)$ a multifractal? If the answer is positive, what is its spectrum of singularities? We consider that these two questions are rather challenging from the numerical and analytical point of view. The results of Section 4 of this paper strongly suggest that the answer to the first question is positive. In fact, we compute $z(t) - c_M t$ for different M and measure the error of the difference between it and an appropriately scaled and rotated version of $\phi(t)$ in the L^∞ norm. The convergence rate is rather strong.

We have also made some numerical experiments that prove that the Hölder exponent of $z(t)$ is $1/2$ for rational times $t_{pq} = (2\pi/M^2)(p/q)$. Nevertheless, how the constants depend of the denominator q, something which is a fundamental ingredient in the arguments in [17] and in [18], is unclear. This question deserves a much more detailed analysis that we plan to make in a forthcoming paper.

In Section 4, we propose a numerical method for (3) and (4). We explain carefully how to take advantage of the symmetries of $\mathbf{X}$ and $\mathbf{T}$ for the types of solutions considered, which leads to a dramatically improvement in the computational cost of the algorithm.

In Section 5, we perform numerical experiments, simulating the evolution of (3) and (4) for different numbers of sides M in the initial polygon. We compare the numerical results with the algebraic values from Section 3, obtaining a complete agreement between both (totally different) approaches. We also analyze carefully the evolution of $\mathbf{X}$, for $s = 0$, giving numerical evidence that ϕ and $z(t)$ in (13) and (15) are intimately connected and, hence, that $z(t)$ is also a multifractal. Finally, we make some comments on the structure of $\mathbf{T}(s,t)$ at a fixed time t_{pq} with $q \gg 1$.

In Section 6, we offer the main conclusions, as well as some open questions that we postpone for the future.

In order to conclude this paper, we offer in Appendix A a detailed study of those aspects of the generalized quadratic Gauß sums that are of relevance for our work.

2. The Hasimoto transformation

A central point of this paper is the natural connection between (3)-(4) and the nonlinear Schrödinger (NLS) equation. Indeed, applying the Hasimoto transformation [22]:

$$\psi(s,t) = c(s,t)\exp\left(i\int_0^s \tau(s',t)ds'\right), \qquad (16)$$

ψ satisfies the equation

$$\psi_t = i\psi_{ss} + i\left(\frac{1}{2}(|\psi|^2 + A(t))\right)\psi, \tag{17}$$

where $A(t)$ is a certain real constant that depends on time. Nevertheless, for our purposes it is not convenient to work with the torsion. Instead, we consider another version of the Frenet-Serret trihedron; it is easy to check that all its possible generalizations have the form

$$\begin{pmatrix} \mathbf{T} \\ \mathbf{e}_1 \\ \mathbf{e}_2 \end{pmatrix}_s = \begin{pmatrix} 0 & \alpha & \beta \\ -\alpha & 0 & \gamma \\ -\beta & -\gamma & 0 \end{pmatrix} \cdot \begin{pmatrix} \mathbf{T} \\ \mathbf{e}_1 \\ \mathbf{e}_2 \end{pmatrix}, \tag{18}$$

for some vectors $\mathbf{e}_1$ and $\mathbf{e}_2$ that form an orthonormal base with $\mathbf{T}$. Moreover, we can make, without loss of generality, one of the coefficients α, β, or γ equal zero. If we make $\beta = 0$, denoting $\alpha \equiv c$ and $\gamma \equiv \tau$, we recover the habitual trihedron. On the other hand, in this paper, we choose $\gamma \equiv 0$, in order to avoid working with the torsion. In that case, the Hasimoto transformation takes the form

$$\psi \equiv \alpha + i\beta. \tag{19}$$

It is quite straightforward to check that this new definition of ψ also satisfies (17). Indeed, defining (see [22])

$$\mathbf{N} \equiv \mathbf{e}_1 + i\mathbf{e}_2, \tag{20}$$

the generalized trihedron becomes

$$\begin{aligned} \mathbf{T}_s &= \frac{1}{2}(\bar{\psi}\mathbf{N} + \psi\bar{\mathbf{N}}) \\ \mathbf{N}_s &= -\psi\mathbf{T}. \end{aligned} \tag{21}$$

Bearing in mind that $\mathbf{T} \wedge \mathbf{N} = -i\mathbf{N}$, (4) gets transformed into

$$\begin{aligned} \mathbf{T}_t &= \mathbf{T} \wedge \left[\frac{1}{2}(\bar{\psi}\mathbf{N} + \psi\bar{\mathbf{N}})\right]_s \\ &= \frac{1}{2}\mathbf{T} \wedge (\bar{\psi}_s\mathbf{N} + \bar{\psi}\mathbf{N}_s + \psi_s\bar{\mathbf{N}} + \psi\bar{\mathbf{N}}_s) \\ &= \frac{i}{2}(\psi_s\bar{\mathbf{N}} - \bar{\psi}_s\mathbf{N}). \end{aligned} \tag{22}$$

We want to express $\mathbf{N}_t$ as $\mathbf{N}_t = a\mathbf{T} + b\mathbf{N} + c\bar{\mathbf{N}}$:

$$\begin{aligned} &\mathbf{N}\cdot\mathbf{T} = 0 \Rightarrow \mathbf{N}_t\cdot\mathbf{T} = -\mathbf{N}\cdot\mathbf{T}_t = -i\psi_s \\ &\mathbf{N}\cdot\mathbf{N} = 0 \Rightarrow \mathbf{N}_t\cdot\mathbf{N} = 0 \\ &\mathbf{N}\cdot\bar{\mathbf{N}} = 2 \Rightarrow \mathbf{N}_t\cdot\bar{\mathbf{N}} + \mathbf{N}\cdot\bar{\mathbf{N}}_t = 0. \end{aligned} \tag{23}$$

From the last equation, it follows that the real part of $\mathbf{N}_t\cdot\bar{\mathbf{N}}$ is equal to zero, so $\mathbf{N}_t\cdot\bar{\mathbf{N}} = iR$, for some $R\in\mathbb{R}$. Putting all together,

$$\mathbf{N}_t = -i\psi_s\mathbf{T} + iR\mathbf{N}. \tag{24}$$

Differentiating this last expression with respect to s,

$$\begin{aligned} \mathbf{N}_{ts} &= (-i\psi_s\mathbf{T} + iR\mathbf{N})_s \\ &= -i\psi_{ss}\mathbf{T} - i\psi_s\mathbf{T}_s + iR_s\mathbf{N} + iR\mathbf{N}_s \\ &= -(i\psi_{ss} + iR\psi)\mathbf{T} - \frac{i}{2}\bar{\psi}\psi_s\mathbf{N} + iR_s\mathbf{N} - \frac{i}{2}\psi\psi_s\bar{\mathbf{N}}. \end{aligned} \tag{25}$$

On the other hand

$$\begin{aligned} \mathbf{N}_{st} &= -(\psi\mathbf{T})_t \\ &= -\psi_t\mathbf{T} - \psi\mathbf{T}_t \\ &= -\psi_t\mathbf{T} + \frac{i}{2}\psi\bar{\psi}_s\mathbf{N} - \frac{i}{2}\psi\psi_s\bar{\mathbf{N}}. \end{aligned} \tag{26}$$

Equating the coefficients of $\mathbf{T}$ and $\mathbf{N}$ in (25) and (26):

$$\begin{aligned} &\psi_t = i\psi_{ss} + iR\psi \\ &R_s = \frac{1}{2}\psi\bar{\psi}_s + \frac{1}{2}\bar{\psi}\psi_s \Longrightarrow R = \frac{1}{2}(|\psi|^2 + A(t)), \quad A(t)\in\mathbb{R}. \end{aligned} \tag{27}$$

This concludes the proof that $\psi = \alpha + i\beta$ satisfies (17).

3. A solution of $\mathbf{X}_t = \mathbf{X}_s \wedge \mathbf{X}_{ss}$ for a regular polygon

The aim of this paper is trying to understand the evolution of (3) for polygonal initial data. In this paper, we limit ourselves to studying the simplest case, i.e., that of a regular planar polygon of M sides. Since (3) and (4) are invariant by rotations, we can assume without loss of generality that $\mathbf{X}(s,0)$, and hence $\mathbf{T}(s,0)$, live in the plane OXY, i.e., their third component is zero. Identifying the plane OXY with $\mathbb{C}$, and assuming without loss of generality a total length of 2π, $\mathbf{X}(s,0)$ is the polygon parameterized by arc-length whose M vertices $s_0,\dots,s_{M-1}$, located at $s_k = 2\pi k/M$, are

$$\mathbf{X}(s_k,0) = \frac{-i\pi e^{i\pi(2k-1)/M}}{M\sin(\pi/M)}, \tag{28}$$

and $\mathbf{X}(s,0)$, for $s_k < s < s_{k+1}$, is in the segment that joints $\mathbf{X}(s_k,0)$ and $\mathbf{X}(s_{k+1},0)$. Observe that it is straightforward to extend $\mathbf{X}(s,0)$ periodically to the whole real with period 2π. Then, since $\mathbf{X}(s_{k+1},0) - \mathbf{X}(s_k,0) = (2\pi/M)e^{2\pi ik/M}$, the corresponding tangent vector is the periodic function with period 2π such that

$$\mathbf{T}(s,0) = e^{2\pi ik/M}, \quad \text{for } s_k < s < s_{k+1}. \tag{29}$$

Remark that $\mathbf{X}(s,0)$ is continuous, while $\mathbf{T}(s,0)$ is only piecewise continuous. In fact, $\mathbf{X}(s,0)$ can be regarded as a curve whose curvature, periodic with period $2\pi/M$, is zero everywhere, except at the vertices, where it equals infinity, i.e., it can be expressed as a sum of Dirac deltas:

$$\kappa(s) = \frac{2\pi}{M}\sum_{k=-\infty}^{\infty}\delta(s - \tfrac{2\pi k}{M}); \tag{30}$$

where the constant $2\pi/M$ has be chosen in order that the integral of the curvature over an interval of length 2π is equal to 2π:

$$\int_{0^-}^{2\pi^-}\kappa(s)ds = \frac{2\pi}{M}\int_{0^-}^{2\pi^-}\left[\sum_{k=0}^{M-1}\delta(s - \tfrac{2\pi k}{M})\right]ds = 2\pi. \tag{31}$$

At this point, it is vital to understand the role played by symmetries in (3) and (4) for this initial datum. Both equations are invariant by rotations, i.e, given a rotation matrix $\mathbf{R}$, if $\mathbf{X} = (X_1,X_2,X_3)^T$ and $\mathbf{T} = (T_1,T_2,T_3)^T$ are, respectively, solutions of them, so are $\mathbf{R}\cdot\mathbf{X}$ and $\mathbf{R}\cdot\mathbf{T}$. Therefore, if $\mathbf{R}\cdot\mathbf{X}(s,0) = \mathbf{X}(s,0)$ and $\mathbf{R}\cdot\mathbf{T}(s,0) = \mathbf{T}(s,0)$, then, if the solution is unique, $\mathbf{R}\cdot\mathbf{X}(s,t) = \mathbf{X}(s,t)$ and $\mathbf{R}\cdot\mathbf{T}(s,t) = \mathbf{T}(s,t)$, $\forall t$. In particular, since $\mathbf{X}(s,0)$ and $\mathbf{T}(s,0)$ defined in (28) and (29) are invariant to rotations of angle $2\pi k/M$, around the z-axis, $\forall k \in \mathbb{Z}$, we conclude that also $\mathbf{X}(s,t)$

and $\mathbf{T}(s,t)$ are invariant to that kind of rotations, $\forall t$. More precisely, writing $\mathbf{X} = (X_1, X_2, X_3)$, $\mathbf{T} = (T_1, T_2, T_3)$, then, $\forall k \in \mathbb{N}$,

$$\begin{aligned} X_1(s + \tfrac{2\pi k}{M}, t) + iX_2(s + \tfrac{2\pi k}{M}, t) &= e^{2\pi ik/M}(X_1(s,t) + iX_2(s,t)), \\ X_3(s + \tfrac{2\pi k}{M}, t) &= X_3(s,t), \\ T_1(s + \tfrac{2\pi k}{M}, t) + iT_2(s + \tfrac{2\pi k}{M}, t) &= e^{2\pi ik/M}(T_1(s,t) + iX_2(T,t)), \\ T_3(s + \tfrac{2\pi k}{M}, t) &= T_3(s,t); \end{aligned} \tag{32}$$

consequently, for a given t, $\mathbf{X}(s + 2\pi k/M, t)$ lay in the same orthogonal plane to the z-axis, $\forall k \in \mathbb{N}$. This fact has very important implications for implementing efficient numerical schemes, as we will see in Section 4.

Besides invariance by rotations, (3) is also mirror invariant. Indeed, it is straightforward to check that, if, for instance, $\mathbf{X}$ is a solution of (3), so is $\tilde{\mathbf{X}}(s,t) = (-X_1(-s,t), X_2(-s,t), X_3(-s,t))^T$, etc. Therefore, if $\tilde{\mathbf{X}}(s,0) = \mathbf{X}(s,0)$, then that symmetry will be again preserved during the evolution, i.e, $\tilde{\mathbf{X}}(s,t) = \mathbf{X}(s,t)$, $\forall t$, or, in other words, $\mathbf{X}(s,t)$ and $\mathbf{X}(-s,t)$ will be symmetric with respect to the plain containing the z-axis and the y-axis, $\forall t$. In our case, we can see immediately that a regular polygon of M sides like (28) has $2M$ of those mirror symmetries. For instance, in Figure 1, we have plotted a pentagon (blue), together with the projections over $z = 0$ of its ten symmetry planes (red). Those symmetry planes are such that they contain the z axis, and one of the points $\mathbf{X}(\pi k/5, 0)$, $k = 0, \ldots, 9$, which are precisely the vertices of the pentagon and the middle points of the sides of the pentagon. Therefore, it follows that $\mathbf{X}(\pi k/5, t)$ will remain in the plane that contains $\mathbf{X}(\pi k/5, 0)$ and the z-axis, $\forall t$. An extremely important corollary that will be used later is that $\mathbf{X}(2\pi/M, t) - \mathbf{X}(0,t)$ is a positive multiple of the vector $(1,0,0)^T$.

Another central point of this paper is the fact that the NLS equation (17) is invariant by the so-called Galilean transformations, i.e., if ψ is a solution of (17), so is

$$\tilde{\psi}_k(s,t) \equiv e^{iks - ik^2 t}\psi(s - 2kt, t), \quad \forall k, t \in \mathbb{R}. \tag{33}$$

Therefore, if we chose an initial datum such that $\tilde{\psi}_k(s,0) = \psi(s,0)$, $\forall k \in \mathbb{R}$, i.e., such that $\psi(s,0) = e^{iks}\psi(s,0)$, $\forall k \in \mathbb{R}$, then, if the solution is unique, $\psi(s,t) = e^{iks - ik^2 t}\psi(s - 2kt, t)$, for $\forall k, t \in \mathbb{R}$.

In the case of a planar initial datum $\mathbf{X}(s,0)$ of (3), the torsion is always equal to zero and, $\psi(s,0)$ is by definition the curvature of $\mathbf{X}(s,0)$. Hence,

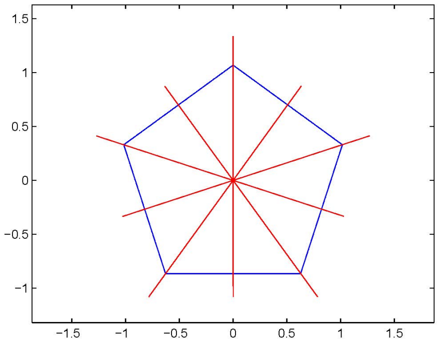

Figure 1: The ten mirror symmetries for a pentagonal initial datum

the $\psi(s,0)$ corresponding to a regular polygon of N sides is given by (30), i.e.,

$$\psi(s,0)=\frac{2\pi}{M}\sum_{k=-\infty}^{\infty}\delta(s-\tfrac{2\pi k}{M}). \tag{34}$$

Like (30), $\psi(s,0)$ is periodic of period $2\pi/M$ and, since (17) is invariant by space translations, $\psi(s,t)$ is also periodic of that period, $\forall t$. Moreover, it satisfies $\psi(s,0)=e^{iMks}\psi(s,0)$, $\forall k\in\mathbb{Z}$. Therefore, the Galilean transformation hold, i.e., $\psi(s,t)=e^{iMks-i(Mk)^2t}\psi(s-2Mkt,t)$, $\forall k\in\mathbb{Z}$, $\forall t\in\mathbb{R}$. Bearing in mind the previous arguments, let us calculate the Fourier coefficients of $\psi(s,t)$:

$$\begin{aligned}
\hat{\psi}(j,t) &= \frac{M}{2\pi}\int_0^{2\pi/M} e^{-iMjs}\psi(s,t)ds \\
&= \frac{M}{2\pi}\int_0^{2\pi/M} e^{-iMjs}\left[e^{iMks-i(Mk)^2t}\psi(s-2Mkt,t)\right]ds \\
&= \frac{Me^{-i(Mk)^2t}}{2\pi}\int_0^{2\pi/M} e^{-iM(j-k)s}\psi(s-2Mkt,t)ds \\
&= \frac{Me^{-i(Mk)^2t}}{2\pi}\int_0^{2\pi/M} e^{-iM(j-k)(s+2Mkt)}\psi(s,t)ds \\
&= \frac{Me^{-i(Mk)^2t-iM(j-k)(2Mkt)}}{2\pi}\int_0^{2\pi/M} e^{-iM(j-k)s}\psi(s,t)ds \\
&= e^{-i(Mk)^2t-iM(j-k)(2Mkt)}\hat{\psi}(j-k,t).
\end{aligned} \tag{35}$$

This identity holds for all j and k. In particular, evaluating both sides at $j = k$:

$$\hat{\psi}(k,t) = e^{-i(Mk)^2 t}\hat{\psi}(0,t), \tag{36}$$

so ψ can be expressed as

$$\psi(s,t) = \hat{\psi}(0,t) \sum_{k=-\infty}^{\infty} e^{-i(Mk)^2 t + iMks}, \tag{37}$$

where $\hat{\psi}(0,t)$ is a constant that depends on time and that has to be chosen in such a way that the corresponding $\mathbf{X}$ and $\mathbf{T}$ are periodic of period 2π for a fixed t; for instance, when $t = 0$, we have trivially $\hat{\psi}(0,0) = 1$. Moreover, combining (34) and (37), we get the following well-known identity:

$$\sum_{k=-\infty}^{\infty} e^{i(Mk)s} \equiv \frac{2\pi}{M} \sum_{k=-\infty}^{\infty} \delta(s - \tfrac{2\pi k}{M}). \tag{38}$$

Observe that, if we solve the linear Schrödinger equation

$$u_t = iu_{xx} \tag{39}$$

for the initial data (34), we get

$$\psi(s,t) = \sum_{k=-\infty}^{\infty} e^{-i(Mk)^2 t + i(Mk)s} = \theta(\tfrac{M}{2\pi}, \tfrac{M^2}{\pi}), \tag{40}$$

where $\theta(s,t)$ is the well-known Jacobi theta function (9). (40) is the same formula as in (37), but with $\hat{\psi}(0,t) \equiv 1$, $\forall t \in \mathbb{R}$. Indeed, obtaining a universal expression for $\hat{\psi}(0,t)$ in the nonlinear case is not an easy problem. Nevertheless, after observing that $e^{-i(Mk)^2 t + i(Mk)s}$ is periodic in time with period $2\pi/M^2$, we have been able to calculate $\hat{\psi}(0,t)$ by algebraic means for rational multiples of $2\pi/M^2$, as is shown in (87). Moreover, that value appears to be unique. Therefore, we give evidence that also $\psi(s,t)$ is periodic in time with period $2\pi/M^2$, strongly suggesting that (4) is also periodic in time with the same period. These considerations are fully supported by numerical simulation.

3.1. $\psi(s,t)$ for rational multiples of $t = 2\pi/M^2$

Let us evaluate (37) at $t = t_{pq} = (2\pi/M^2)(p/q)$, where $p \in \mathbb{Z}$, $q \in \mathbb{N}$, and we can suppose without loss of generality that $\gcd(p,q) = 1$:

$$\begin{aligned}
\psi(s,t_{pq}) &= \hat{\psi}(0,t_{pq}) \sum_{k=-\infty}^{\infty} e^{-i(Mk)^2 2\pi p/(M^2 q) + iMks} \\
&= \hat{\psi}(0,t_{pq}) \sum_{k=-\infty}^{\infty} e^{-2\pi i (p/q) k^2 + iMks} \\
&= \hat{\psi}(0,t_{pq}) \sum_{l=0}^{q-1} \sum_{k=-\infty}^{\infty} e^{-2\pi i (p/q)(qk+l)^2 + iM(qk+l)s} \\
&= \hat{\psi}(0,t_{pq}) \sum_{l=0}^{q-1} e^{-2\pi i (p/q) l^2 + iMls} \sum_{k=-\infty}^{\infty} e^{iMqks}. \qquad (41)
\end{aligned}$$

Using the identity (38),

$$\begin{aligned}
\psi(s,t_{pq}) &= \frac{2\pi}{Mq} \hat{\psi}(0,t_{pq}) \sum_{l=0}^{q-1} e^{-2\pi i (p/q) l^2 + iMls} \sum_{k=-\infty}^{\infty} \delta(s - \tfrac{2\pi k}{Mq}) \\
&= \frac{2\pi}{Mq} \hat{\psi}(0,t_{pq}) \sum_{l=0}^{q-1} \sum_{k=-\infty}^{\infty} e^{-2\pi i (p/q) l^2 + iMl(2\pi k/Mq)} \delta(s - \tfrac{2\pi k}{Mq}) \\
&= \frac{2\pi}{Mq} \hat{\psi}(0,t_{pq}) \sum_{k=-\infty}^{\infty} \sum_{l=0}^{q-1} e^{-2\pi i (p/q) l^2 + 2\pi i (k/q) l} \delta(s - \tfrac{2\pi k}{Mq}) \\
&= \frac{2\pi}{Mq} \hat{\psi}(0,t_{pq}) \sum_{k=-\infty}^{\infty} \sum_{m=0}^{q-1} \sum_{l=0}^{q-1} e^{-2\pi i (p/q) l^2 + 2\pi i (m/q) l} \delta(s - \tfrac{2\pi k}{M} - \tfrac{2\pi m}{Mq}) \\
&= \frac{2\pi}{Mq} \hat{\psi}(0,t_{pq}) \sum_{k=-\infty}^{\infty} \sum_{m=0}^{q-1} G(-p,m,q) \delta(s - \tfrac{2\pi k}{M} - \tfrac{2\pi m}{Mq}), \qquad (42)
\end{aligned}$$

where

$$G(a,b,c) = \sum_{l=0}^{c-1} e^{2\pi i (al^2 + bl)/c}, \quad a,b \in \mathbb{Z}, c \in \mathbb{Z} - \{0\}, \qquad (43)$$

denotes a generalized quadratic Gauß sum. In Appendix A, we give all the information about these sums relevant for this paper; in particular, we show that, if $\gcd(p,q)=1$, then

$$|G(-p,m,q)| = \begin{cases} \sqrt{q}, & \text{if } q \text{ is odd}, \\ \sqrt{2q}, & \text{if } q \text{ is even and } q/2 \equiv m \mod 2, \\ 0, & \text{if } q \text{ is even and } q/2 \not\equiv m \mod 2. \end{cases} \tag{44}$$

Therefore, $\psi(s,t)$ has evolved from M Dirac deltas in $[0,2\pi)$ at $t=0$, to Mq deltas in $[0,2\pi)$ at t_{pq}, for q odd; and $Mq/2$ deltas in $[0,2\pi)$ at t_{pq}, for q even. Furthermore, from (44),

$$G(-p,m,q) = \begin{cases} \sqrt{q}e^{i\theta_m}, & \text{if } q \text{ is odd}, \\ \sqrt{2q}e^{i\theta_m}, & \text{if } q \text{ is even and } q/2 \equiv m \mod 2, \\ 0, & \text{if } q \text{ is even and } q/2 \not\equiv m \mod 2, \end{cases} \tag{45}$$

for a certain angle θ_m that depends on m (and, of course, on p and q, too). Introducing (45) into (42), and restricting ourselves to $k=0$, i.e., $[0,\frac{2\pi}{M})$, we conclude that

$$\psi(s,t_{pq}) = \begin{cases} \frac{2\pi}{M\sqrt{q}}\hat{\psi}(0,t_{pq})\sum_{m=0}^{q-1} e^{i\theta_m}\delta(s-\frac{2\pi m}{Mq}), & \text{if } q \text{ odd}, \\ \frac{2\pi}{M\sqrt{\frac{q}{2}}}\hat{\psi}(0,t_{pq})\sum_{m=0}^{q/2-1} e^{i\theta_{2m+1}}\delta(s-\frac{4\pi m+2\pi}{Mq}), & \text{if } q/2 \text{ odd}, \\ \frac{2\pi}{M\sqrt{\frac{q}{2}}}\hat{\psi}(0,t_{pq})\sum_{m=0}^{q/2-1} e^{i\theta_{2m}}\delta(s-\frac{4\pi m}{Mq}), & \text{if } q/2 \text{ even}. \end{cases} \tag{46}$$

The coefficients multiplying the Dirac deltas are in general not real, except for $t=0$ and $t_{1,2}=\pi/M^2$. Therefore, $\psi(s,t_{pq})$ does not correspond to a planar polygon, but to a skew polygon with Mq sides, for q odd; and to a skew polygon with $Mq/2$ sides, for q even. Moreover, $\hat{\psi}(0,t_{pq})$ has to be determined in such a way that the polygon is closed; this is done in the next section, where we show that its rather involved choice is unique, concluding that $\psi(s,t)$ is periodic in time, with period $2\pi/M^2$.

Since the Dirac deltas are equally spaced at a time $t=t_{pq}$, the length of the sides is the same. Observe that, if $q/2$ is odd, i.e., if $q\equiv 2 \mod 4$, then there is no vertex at $s=0$. For instance, if $p=1$, $q=2$, i.e., $t=\pi/M^2$, then

$$\psi(s,t_{1,2}) = \frac{2\pi}{M}\sum_{k=-\infty}^{\infty}\delta(s-\tfrac{2\pi(2k+1)}{2M}). \tag{47}$$

Furthermore, the coefficients multiplying the Dirac deltas are now real, so $\psi(s,t_{1,2})$ is simply the curvature, and $\psi(0,t_{1,2})=1$ has been chosen in order that the integral of $\psi(s, t_{1,2})$ over $[0, 2\pi)$ is 2π. Bearing in mind the symmetries of the problem, we conclude that the corresponding polygon is a regular planar polygon of M sides, which lives at a certain plane $z = \text{constant}$, and which has been rotated π/M degrees around the z-axis with respect to the initial data, as R. Jerrard and D. Smets predicted.

3.2. Recovering $\mathbf{X}$ *and* $\mathbf{T}$ *from* ψ *at* $t = t_{pq}$

Given $\psi(s,t) = \alpha(s,t) + i\beta(s,t)$, recovering $\mathbf{T}$, $\mathbf{e}_1$ and $\mathbf{e}_2$ from ψ implies integrating

$$\begin{pmatrix} \mathbf{T} \\ \mathbf{e}_1 \\ \mathbf{e}_2 \end{pmatrix}_s = \begin{pmatrix} 0 & \alpha & \beta \\ -\alpha & 0 & 0 \\ -\beta & 0 & 0 \end{pmatrix} \cdot \begin{pmatrix} \mathbf{T} \\ \mathbf{e}_1 \\ \mathbf{e}_2 \end{pmatrix}. \tag{48}$$

As we have seen in the previous section, at a time $t_{pq} = (2\pi/M^2)(p/q)$, $\psi(s, t_{pq})$ is a sum of Mq (if q odd) or $Mq/2$ (if q even) equally spaced Dirac deltas, that corresponds to a skew polygon $\mathbf{X}(s, t_{pq})$ of Mq or $Mq/2$ sides. To integrate (48), we have to understand the transition from one side of the polygon to the next one. In order to do that, we reduce ourselves, without loss of generality, to a certain ψ formed by a single Dirac delta located at $s = 0$, i.e, $\psi(s) = (a + ib)\delta(s)$, so we have to integrate

$$\begin{pmatrix} \mathbf{T} \\ \mathbf{e}_1 \\ \mathbf{e}_2 \end{pmatrix}_s = \begin{pmatrix} 0 & a\delta & b\delta \\ -a\delta & 0 & 0 \\ -b\delta & 0 & 0 \end{pmatrix} \cdot \begin{pmatrix} \mathbf{T} \\ \mathbf{e}_1 \\ \mathbf{e}_2 \end{pmatrix}. \tag{49}$$

This system corresponds to some $\mathbf{T}(s)$, $\mathbf{e}_1(s)$ and $\mathbf{e}_2(s)$ constant, except at $s = 0$, where there is a singularity. Let us suppose that, for $s < 0$, $\mathbf{T}(s) \equiv \mathbf{T}(0^-)$, $\mathbf{e}_1(s) \equiv \mathbf{e}_1(0^-)$, $\mathbf{e}_2(s) \equiv \mathbf{e}_2(0^-)$, so we want to calculate $\mathbf{T}(0^+)$, $\mathbf{e}_1(0^+)$, $\mathbf{e}_2(0^+)$, such that, for $s > 0$, $\mathbf{T}(s) \equiv \mathbf{T}(0^+)$, $\mathbf{e}_1(s) \equiv \mathbf{e}_1(0^+)$, $\mathbf{e}_2(s) \equiv \mathbf{e}_2(0^+)$. In this case, the problem is equivalent to that one of a plane curve with curvature κ the delta function at one point, $\kappa(s) = a\delta(s)$; therefore, it is equivalent to solving

$$\begin{pmatrix} \mathbf{T} \\ \mathbf{n} \end{pmatrix}_s = \begin{pmatrix} 0 & a\delta \\ -a\delta & 0 \end{pmatrix} \cdot \begin{pmatrix} \mathbf{T} \\ \mathbf{n} \end{pmatrix}. \tag{50}$$

The correct way to understand (50) is to write it as

$$\left(e^{i\int_0^s \kappa(s')ds'} z'(s)\right)' = \left(e^{ia\int_0^s \delta(s')ds'} z'(s)\right)' = 0, \tag{51}$$

with $z(s) = x(s) + iy(s)$ the parametrization of the curve with arc-length parameter s.

In order to integrate (49), it is important to notice that, although $\mathbf{T}$, $\mathbf{e}_1$ and $\mathbf{e}_2$ are vectors, it can be uncoupled into three systems of ODE's for $(T_1, e_{1,1}, e_{2,1})$, $(T_2, e_{1,2}, e_{2,2})$ and $(T_3, e_{1,3}, e_{2,3})$, respectively. Hence, let us consider

$$\begin{pmatrix} u_1 \\ u_2 \\ u_3 \end{pmatrix}_s = \begin{pmatrix} 0 & a\delta & b\delta \\ -a\delta & 0 & 0 \\ -b\delta & 0 & 0 \end{pmatrix} \cdot \begin{pmatrix} u_1 \\ u_2 \\ u_3 \end{pmatrix} = \delta(s) \begin{pmatrix} 0 & a & b \\ -a & 0 & 0 \\ -b & 0 & 0 \end{pmatrix} \cdot \begin{pmatrix} u_1 \\ u_2 \\ u_3 \end{pmatrix}. \tag{52}$$

Then, motivated by (51), we proceed as in the case of a plane curve:

$$\begin{aligned} \begin{pmatrix} u_1(0^+) \\ u_2(0^+) \\ u_3(0^+) \end{pmatrix} &= \exp\left[\begin{pmatrix} 0 & a & b \\ -a & 0 & 0 \\ -b & 0 & 0 \end{pmatrix} \int_{0^-}^{0^+} \delta(s')ds' \right] \cdot \begin{pmatrix} u_1(0^-) \\ u_2(0^-) \\ u_3(0^-) \end{pmatrix} \\ &= \exp\left[\begin{pmatrix} 0 & a & b \\ -a & 0 & 0 \\ -b & 0 & 0 \end{pmatrix} \right] \cdot \begin{pmatrix} u_1(0^-) \\ u_2(0^-) \\ u_3(0^-) \end{pmatrix}. \end{aligned} \tag{53}$$

We can compute explicitly the matrix exponential:

$$\exp(\mathbf{A}) = \begin{pmatrix} \cos(\sqrt{a^2 + b^2}) & \frac{a \sin(\sqrt{a^2+b^2})}{\sqrt{a^2+b^2}} & \frac{b \sin(\sqrt{a^2+b^2})}{\sqrt{a^2+b^2}} \\ \frac{-a \sin(\sqrt{a^2+b^2})}{\sqrt{a^2+b^2}} & \frac{a^2 \cos(\sqrt{a^2+b^2})+b^2}{a^2+b^2} & \frac{ab \cos(\sqrt{a^2+b^2})-ab}{a^2+b^2} \\ \frac{-b \sin(\sqrt{a^2+b^2})}{\sqrt{a^2+b^2}} & \frac{ab \cos(\sqrt{a^2+b^2})-ab}{a^2+b^2} & \frac{b^2 \cos(\sqrt{a^2+b^2})+a^2}{a^2+b^2} \end{pmatrix}. \tag{54}$$

Furthermore, this matrix can be rewritten in a much more elegant way. Indeed, expressing $a + ib$ in polar form, i.e., $a + ib \equiv \rho e^{i\theta}$, then

$$\exp(\mathbf{A}) = \begin{pmatrix} \cos(\rho) & \sin(\rho)\cos(\theta) & \sin(\rho)\sin(\theta) \\ -\sin(\rho)\cos(\theta) & \cos(\rho)\cos^2(\theta) + \sin^2(\theta) & [\cos(\rho) - 1]\cos(\theta)\sin(\theta) \\ -\sin(\rho)\sin(\theta) & [\cos(\rho) - 1]\cos(\theta)\sin(\theta) & \cos(\rho)\sin^2(\theta) + \cos^2(\theta) \end{pmatrix} \tag{55}$$

$$\begin{aligned} &= \mathbf{I} + \sin(\rho) \begin{pmatrix} 0 & \cos(\theta) & \sin(\theta) \\ -\cos(\theta) & 0 & 0 \\ -\sin(\theta) & 0 & 0 \end{pmatrix} \\ &\quad + (1 - \cos(\rho)) \begin{pmatrix} -1 & 0 & 0 \\ 0 & -\cos^2(\theta) & -\cos(\theta)\sin(\theta) \\ 0 & -\cos(\theta)\sin(\theta) & -\sin^2(\theta) \end{pmatrix}. \end{aligned} \tag{56}$$

Hence, $\exp(\mathbf{A})$ is a rotation matrix [23], because $\exp(\mathbf{A})^T \cdot \exp(\mathbf{A}) = \mathbf{I}$. More precisely, it is the rotation matrix corresponding to a rotation about an axis

$(0, \sin(\theta), -\cos(\theta))$ by an angle ρ. $\exp(\mathbf{A})$ also relates $\{\mathbf{T}(0^-), \mathbf{e}_1(0^-), \mathbf{e}_2(0^-)\}$ and $\{\mathbf{T}(0^+), \mathbf{e}_1(0^+), \mathbf{e}_2(0^+)\}$:

$$\left(\begin{array}{c} \mathbf{T}(0^+)^T \\ \hline \mathbf{e}_1(0^+)^T \\ \hline \mathbf{e}_2(0^+)^T \end{array}\right) = \exp(\mathbf{A}) \cdot \left(\begin{array}{c} \mathbf{T}(0^-)^T \\ \hline \mathbf{e}_1(0^-)^T \\ \hline \mathbf{e}_2(0^-)^T \end{array}\right). \tag{57}$$

Therefore, if $\{\mathbf{T}(0^-), \mathbf{e}_1(0^-), \mathbf{e}_2(0^-)\}$ forms an orthonormal basis of $\mathbb{R}^3$, so does $\{\mathbf{T}(0^+), \mathbf{e}_1(0^+), \mathbf{e}_2(0^+)\}$.

Coming back to the general form of ψ, we have to integrate (52) Mq or $Mq/2$ times to obtain a closed skew, i.e., non-planar polygon with Mq or $Mq/2$ sides. But, according to (46), in $[0, \frac{2\pi}{M})$,

$$\psi(s, t_{pq}) = \begin{cases} \sum_{m=0}^{q-1} (\alpha_m + i\beta_m)\delta(s - \frac{2\pi m}{Mq}), & \text{if } q \text{ odd}, \\ \sum_{m=0}^{q/2-1} (\alpha_{2m+1} + i\beta_{2m+1})\delta(s - \frac{4\pi m + 2\pi}{Mq}), & \text{if } q/2 \text{ odd}, \\ \sum_{m=0}^{q/2-1} (\alpha_{2m} + i\beta_{2m})\delta(s - \frac{4\pi m}{Mq}), & \text{if } q/2 \text{ even}, \end{cases} \tag{58}$$

where

$$|\alpha_m + i\beta_m| = \rho = \begin{cases} \frac{2\pi}{M\sqrt{q}} \hat{\psi}(0, t_{pq}), & \text{if } q \text{ is odd}, \\ \frac{2\pi}{M\sqrt{\frac{q}{2}}} \hat{\psi}(0, t_{pq}), & \text{if } q \text{ is even and } q/2 \equiv m \mod 2, \\ 0, & \text{if } q \text{ is even and } q/2 \not\equiv m \mod 2, \end{cases} \tag{59}$$

so we conclude that, at any time t_{pq}, the angle ρ between two adjacent sides is constant. Furthermore, the structure of the polygon is completely determined by the angles θ_m appearing in the generalized quadratic Gaussian sum, where $\alpha_m + i\beta_m = \rho e^{i\theta_m}$.

Let be $\mathbf{M}_m$ the rotation matrix corresponding to $(\alpha_m + i\beta_m)\delta$. If $\alpha_m + i\beta_m \equiv 0$, $\mathbf{M}_m$ is simply an identity matrix and can be ignored. Otherwise, from (55),

$$\mathbf{M}_m = \begin{pmatrix} \cos(\rho) & \sin(\rho)\cos(\theta_m) & \sin(\rho)\sin(\theta_m) \\ -\sin(\rho)\cos(\theta_m) & \cos(\rho)\cos^2(\theta_m) + \sin^2(\theta_m) & [\cos(\rho) - 1]\cos(\theta_m)\sin(\theta_m) \\ -\sin(\rho)\sin(\theta_m) & [\cos(\rho) - 1]\cos(\theta_m)\sin(\theta_m) & \cos(\rho)\sin^2(\theta_m) + \cos^2(\theta_m) \end{pmatrix}. \tag{60}$$

If, for instance, q is odd, bearing in mind that $\mathbf{T}$, $\mathbf{e}_1$ and $\mathbf{e}_2$ are piecewise constant, we have

$$\left(\begin{array}{c}\mathbf{T}(\frac{2\pi}{Mq}^{-})^T\\ \hline \mathbf{e}_1(\frac{2\pi}{Mq}^{-})^T\\ \hline \mathbf{e}_2(\frac{2\pi}{Mq}^{-})^T\end{array}\right) = \left(\begin{array}{c}\mathbf{T}(0^{+})^T\\ \hline \mathbf{e}_1(0^{+})^T\\ \hline \mathbf{e}_2(0^{+})^T\end{array}\right) = \mathbf{M}_0 \cdot \left(\begin{array}{c}\mathbf{T}(0^{-})^T\\ \hline \mathbf{e}_1(0^{-})^T\\ \hline \mathbf{e}_2(0^{-})^T\end{array}\right)$$

$$\left(\begin{array}{c}\mathbf{T}(\frac{4\pi}{Mq}^{-})^T\\ \hline \mathbf{e}_1(\frac{4\pi}{Mq}^{-})^T\\ \hline \mathbf{e}_2(\frac{4\pi}{Mq}^{-})^T\end{array}\right) = \left(\begin{array}{c}\mathbf{T}(\frac{2\pi}{Mq}^{+})^T\\ \hline \mathbf{e}_1(\frac{2\pi}{Mq}^{+})^T\\ \hline \mathbf{e}_2(\frac{2\pi}{Mq}^{+})^T\end{array}\right) = \mathbf{M}_1 \cdot \left(\begin{array}{c}\mathbf{T}(\frac{2\pi}{Mq}^{-})^T\\ \hline \mathbf{e}_1(\frac{2\pi}{Mq}^{-})^T\\ \hline \mathbf{e}_2(\frac{2\pi}{Mq}^{-})^T\end{array}\right)$$

$$\left(\begin{array}{c}\mathbf{T}(\frac{6\pi}{Mq}^{-})^T\\ \hline \mathbf{e}_1(\frac{6\pi}{Mq}^{-})^T\\ \hline \mathbf{e}_2(\frac{6\pi}{Mq}^{-})^T\end{array}\right) = \left(\begin{array}{c}\mathbf{T}(\frac{4\pi}{Mq}^{+})^T\\ \hline \mathbf{e}_1(\frac{4\pi}{Mq}^{+})^T\\ \hline \mathbf{e}_2(\frac{4\pi}{Mq}^{+})^T\end{array}\right) = \mathbf{M}_2 \cdot \left(\begin{array}{c}\mathbf{T}(\frac{4\pi}{Mq}^{-})^T\\ \hline \mathbf{e}_1(\frac{4\pi}{Mq}^{-})^T\\ \hline \mathbf{e}_2(\frac{4\pi}{Mq}^{-})^T\end{array}\right),$$

and so forth, i.e., there is a jump at $s = \frac{2\pi k}{Mq}$. This is equivalent to writing

$$\left(\begin{array}{c}\mathbf{T}(\frac{2\pi k}{Mq}^{+})^T\\ \hline \mathbf{e}_1(\frac{2\pi k}{Mq}^{+})^T\\ \hline \mathbf{e}_2(\frac{2\pi k}{Mq}^{+})^T\end{array}\right) = \mathbf{M}_k \cdot \mathbf{M}_{k-1} \cdot \ldots \mathbf{M}_1 \cdot \mathbf{M}_0 \cdot \left(\begin{array}{c}\mathbf{T}(0^{-})^T\\ \hline \mathbf{e}_1(0^{-})^T\\ \hline \mathbf{e}_2(0^{-})^T\end{array}\right), \tag{61}$$

where $k \in \mathbb{Z}^+$, and $\mathbf{M}_k$ is periodic modulo q, i.e., $\mathbf{M}_{k+q} \equiv \mathbf{M}_k$. This formula is also valid for q even, provided that we bear in mind that half of the $\mathbf{M}_k$ matrices are simply identity matrices. More precisely, for $q \equiv 0 \mod 4$, then

$$\left(\begin{array}{c}\mathbf{T}(\frac{4\pi k}{Mq}^{+})^T\\ \hline \mathbf{e}_1(\frac{4\pi k}{Mq}^{+})^T\\ \hline \mathbf{e}_2(\frac{4\pi k}{Mq}^{+})^T\end{array}\right) = \mathbf{M}_{2k} \cdot \mathbf{M}_{2k-2} \cdot \ldots \mathbf{M}_2 \cdot \mathbf{M}_0 \cdot \left(\begin{array}{c}\mathbf{T}(0^{-})^T\\ \hline \mathbf{e}_1(0^{-})^T\\ \hline \mathbf{e}_2(0^{-})^T\end{array}\right), \tag{62}$$

$\forall k \in \mathbb{Z}^+$. In this case, the matrices with odd subscript are identity matrices, and

$$\left(\begin{array}{c}\mathbf{T}(\frac{4\pi k+2\pi}{Mq}^{+})^T\\ \hline \mathbf{e}_1(\frac{4\pi k+2\pi}{Mq}^{+})^T\\ \hline \mathbf{e}_2(\frac{4\pi k+2\pi}{Mq}^{+})^T\end{array}\right) \equiv \left(\begin{array}{c}\mathbf{T}(\frac{4\pi k+2\pi}{Mq}^{-})^T\\ \hline \mathbf{e}_1(\frac{4\pi k+2\pi}{Mq}^{-})^T\\ \hline \mathbf{e}_2(\frac{4\pi k+2\pi}{Mq}^{-})^T\end{array}\right) \equiv \left(\begin{array}{c}\mathbf{T}(\frac{4\pi k}{Mq}^{+})^T\\ \hline \mathbf{e}_1(\frac{4\pi k}{Mq}^{+})^T\\ \hline \mathbf{e}_2(\frac{4\pi k}{Mq}^{+})^T\end{array}\right). \tag{63}$$

Equivalently, if $q \equiv 2 \mod 4$, then

$$\left(\begin{array}{c}\mathbf{T}(\frac{4\pi k-2\pi}{Mq}^{+})^T\\ \hline \mathbf{e}_1(\frac{4\pi k-2\pi}{Mq}^{+})^T\\ \hline \mathbf{e}_2(\frac{4\pi k-2\pi}{Mq}^{+})^T\end{array}\right) = \mathbf{M}_{2k+1} \cdot \mathbf{M}_{2k-1} \cdot \ldots \mathbf{M}_3 \cdot \mathbf{M}_1 \cdot \left(\begin{array}{c}\mathbf{T}(\frac{2\pi}{Mq}^{-})^T\\ \hline \mathbf{e}_1(\frac{2\pi}{Mq}^{-})^T\\ \hline \mathbf{e}_2(\frac{2\pi}{Mq}^{-})^T\end{array}\right), \tag{64}$$

$\forall k \in \mathbb{Z}^+$. In this case, the matrices with even subscript are identity matrices, and

$$\left(\begin{array}{c}\mathbf{T}(\frac{4\pi k}{Mq}^+)^T\\ \hline \mathbf{e}_1(\frac{4\pi k}{Mq}^+)^T\\ \hline \mathbf{e}_2(\frac{4\pi k}{Mq}^+)^T\end{array}\right) \equiv \left(\begin{array}{c}\mathbf{T}(\frac{4\pi k}{Mq}^-)^T\\ \hline \mathbf{e}_1(\frac{4\pi k}{Mq}^-)^T\\ \hline \mathbf{e}_2(\frac{4\pi k}{Mq}^-)^T\end{array}\right) = \left(\begin{array}{c}\mathbf{T}(\frac{4\pi k-2\pi}{Mq}^+)^T\\ \hline \mathbf{e}_1(\frac{4\pi k-2\pi}{Mq}^+)^T\\ \hline \mathbf{e}_2(\frac{4\pi k-2\pi}{Mq}^+)^T\end{array}\right). \tag{65}$$

When q is even, (63) and (65) explain why the polygon has $q/2$ sides. Equivalently, it could be regarded as having q sides, but half of them being indistinguishable, because when the angle between two adjacent sides is zero, they merge into a single side.

In order that the polygon is closed, we have to choose ρ in (59) in such a way that $\mathbf{T}$, $\mathbf{e}_1$ and $\mathbf{e}_2$ are periodic, i.e.,

$$\left(\begin{array}{c}\mathbf{T}(2\pi^-)^T\\ \hline \mathbf{e}_1(2\pi^-)^T\\ \hline \mathbf{e}_2(2\pi^-)^T\end{array}\right) = \left(\begin{array}{c}\mathbf{T}(0^-)^T\\ \hline \mathbf{e}_1(0^-)^T\\ \hline \mathbf{e}_2(0^-)^T\end{array}\right), \tag{66}$$

which is equivalent to imposing that

$$\mathbf{M}_{Mq-1} \cdot \mathbf{M}_{Mq-2} \cdot \ldots \cdot \mathbf{M}_1 \cdot \mathbf{M}_0 \equiv \mathbf{I}. \tag{67}$$

Let us define

$$\mathbf{M} = \mathbf{M}_{q-1} \cdot \mathbf{M}_{q-2} \cdot \ldots \cdot \mathbf{M}_1 \cdot \mathbf{M}_0. \tag{68}$$

From (67), $\mathbf{M}$ is an M-th root of the identity matrix. Moreover, it is also a rotation matrix that induces a rotation of $2\pi/M$ degrees around a certain rotation axis. Therefore, we have to choose ρ in order that any of the following properties is satisfied:

$$\mathrm{Tr}(\mathbf{M}) = 1 + 2\cos(\tfrac{2\pi}{M}), \tag{69}$$

$$\lambda(\mathbf{M}) = \{1, e^{2\pi i/M}, e^{-2\pi i/M}\}, \tag{70}$$

were $\mathrm{Tr}(\mathbf{M})$ and $\lambda(\mathbf{M})$ denote the trace and the spectrum of $\mathbf{M}$, respectively. We work with the trace, because it is algebraically easier. In order to understand its structure, we analyze a few cases. Let us start with q odd. The angles corresponding to the generalized quadratic Gauß sums for the simplest case, $q = 3$, are

$$\begin{array}{llll} p = 1: & \theta_0 = -\frac{\pi}{2}, & \theta_1 = \frac{\pi}{6}, & \theta_2 = \frac{\pi}{6}, \\ p = 2: & \theta_0 = \frac{\pi}{2}, & \theta_1 = -\frac{\pi}{6}, & \theta_2 = -\frac{\pi}{6}. \end{array} \tag{71}$$

Bearing in mind that $\mathbf{M} = \mathbf{M}_2 \cdot \mathbf{M}_1 \cdot \mathbf{M}_0$, a symbolic manipulator yields for both $p = 1$ and $p = 2$ the following expression:

$$\operatorname{Tr}(\mathbf{M}) = \frac{(1 + \cos(\rho))^3}{2} - 1 = 1 + 2\cos(\tfrac{2\pi}{M}), \tag{72}$$

so the only possible real value for $\cos(\rho)$ is

$$\cos(\rho) = (4 + 4\cos(\tfrac{2\pi}{M}))^{1/3} - 1 = 2\cos^{2/3}(\tfrac{\pi}{M}) - 1. \tag{73}$$

Notice that we arrive at the same conclusion if we impose that $\zeta = e^{2\pi i/M}$ is an eigenvalue of $\mathbf{M}$, i.e., if $\det(\mathbf{M} - \zeta\mathbf{I}) = 0$:

$$\begin{aligned} 0 &= \det(\mathbf{M} - \zeta\mathbf{I}) \\ &= \frac{\zeta^2 - \zeta}{2}(\cos^3(\rho) + 3\cos^2(\rho) + 3\cos(\rho) - 2\zeta - 3 - 2\zeta^{-1}) \\ &= \frac{\zeta^2 - \zeta}{2}((1 + \cos(\rho))^3 - 2\zeta - 4 - 2\zeta^{-1}). \end{aligned} \tag{74}$$

Hence,

$$\begin{aligned} \cos(\rho) &= (2\zeta + 2\zeta^{-1} + 4)^{1/3} - 1 \\ &= (2e^{2\pi i/M} + 2e^{-2\pi i/M} + 4)^{1/3} - 1 \\ &= (4 + 4\cos(\tfrac{2\pi}{M}))^{1/3} - 1 \\ &= 2\cos^{2/3}(\tfrac{\pi}{M}) - 1. \end{aligned} \tag{75}$$

Let us consider now the case $q = 5$. Its corresponding angles are:

$$\begin{array}{llllll} p = 1: & \theta_0 = 0, & \theta_1 = -\frac{2\pi}{5}, & \theta_2 = \frac{2\pi}{5} & \theta_3 = \frac{2\pi}{5}, & \theta_4 = -\frac{2\pi}{5}, \\ p = 2: & \theta_0 = -\pi, & \theta_1 = -\frac{\pi}{5}, & \theta_2 = \frac{\pi}{5} & \theta_3 = \frac{\pi}{5}, & \theta_4 = -\frac{\pi}{5}, \\ p = 3: & \theta_0 = -\pi, & \theta_1 = \frac{\pi}{5}, & \theta_2 = -\frac{\pi}{5} & \theta_3 = -\frac{\pi}{5}, & \theta_4 = \frac{\pi}{5}, \\ p = 4: & \theta_0 = 0, & \theta_1 = \frac{2\pi}{5}, & \theta_2 = -\frac{2\pi}{5} & \theta_3 = -\frac{2\pi}{5}, & \theta_4 = \frac{2\pi}{5}. \end{array} \tag{76}$$

Then, $\mathbf{M} = \mathbf{M}_4 \cdot \mathbf{M}_3 \cdot \mathbf{M}_2 \cdot \mathbf{M}_1 \cdot \mathbf{M}_0$, and, for the four values of p,

$$\operatorname{Tr}(\mathbf{M}) = \frac{(1 + \cos(\rho))^5}{8} - 1 = 1 + 2\cos(\tfrac{2\pi}{M}), \tag{77}$$

so the only possible real value for $\cos(\rho)$ is

$$\cos(\rho) = (16 + 16\cos(\tfrac{2\pi}{M}))^{1/5} - 1 = 2\cos^{2/5}(\tfrac{\pi}{M}) - 1. \tag{78}$$

When q is even, the previous ideas are completely valid. As we saw in the previous section, the case $p = 1$, $q = 2$ is trivial, so let us consider $q = 4$. Then, we have the following angles:

$$\begin{array}{lll} p=1: & \theta_0 = -\frac{\pi}{4}, & \theta_2 = \frac{\pi}{4}, \\ p=3: & \theta_0 = \frac{\pi}{4}, & \theta_2 = -\frac{\pi}{4}. \end{array} \tag{79}$$

$\mathbf{M}_1$ and $\mathbf{M}_3$ are identity matrices, so $\mathbf{M} = \mathbf{M}_2 \cdot \mathbf{M}_0$. Then, for both values of p,

$$\mathrm{Tr}(\mathbf{M}) = (1+\cos(\rho))^2 - 1 = 1 + 2\cos(\tfrac{2\pi}{M}). \tag{80}$$

In this case, $\cos(\rho)$ can take two real values, $\cos(\rho) = \pm(2+2\cos(\frac{2\pi}{M}))^{1/2} - 1$, but, since ρ is real, $|\cos(\rho)| \leq 1$, so the only valid value for $\cos(\rho)$ is

$$\cos(\rho) = (2+2\cos(\tfrac{2\pi}{M}))^{1/2} - 1 = 2\cos(\tfrac{\pi}{M}) - 1. \tag{81}$$

If we now choose $q = 6$, then

$$\begin{array}{llll} p=1: & \theta_1 = -\frac{\pi}{6}, & \theta_3 = \frac{\pi}{2}, & \theta_5 = -\frac{\pi}{6}, \\ p=5: & \theta_1 = \frac{\pi}{6}, & \theta_3 = -\frac{\pi}{2}, & \theta_5 = \frac{\pi}{6}. \end{array} \tag{82}$$

This angles are exactly the same as in (71), but in a different order. Now $\mathbf{M}_0$, $\mathbf{M}_2$ and $\mathbf{M}_4$ are identity matrices; $\mathbf{M} = \mathbf{M}_5 \cdot \mathbf{M}_3 \cdot \mathbf{M}_1$, and the only possible real value for $\cos(\rho)$ is again (73).

Finally, if we choose $q = 8$, then

$$\begin{array}{lllll} p=1: & \theta_0 = -\frac{\pi}{4}, & \theta_2 = 0, & \theta_4 = \frac{3\pi}{4} & \theta_6 = 0, \\ p=3: & \theta_0 = \frac{3\pi}{4}, & \theta_2 = 0, & \theta_4 = -\frac{\pi}{4} & \theta_6 = 0, \\ p=5: & \theta_0 = \frac{3\pi}{4}, & \theta_2 = 0, & \theta_4 = -\frac{\pi}{4} & \theta_6 = 0, \\ p=7: & \theta_0 = -\frac{\pi}{4}, & \theta_2 = 0, & \theta_4 = \frac{3\pi}{4} & \theta_6 = 0. \end{array} \tag{83}$$

$\mathbf{M}_1$, $\mathbf{M}_3$, $\mathbf{M}_5$ and $\mathbf{M}_7$ are identity matrices, so $\mathbf{M} = \mathbf{M}_6 \cdot \mathbf{M}_4 \cdot \mathbf{M}_2 \cdot \mathbf{M}_0$. Then, for all the possible values of p we have

$$\mathrm{Tr}(\mathbf{M}) = \frac{(1+\cos(\rho))^4}{4} - 1 = 1 + 2\cos(\tfrac{2\pi}{M}), \tag{84}$$

and the only real value that satisfies $|\cos(\rho)| \leq 1$ is:

$$\cos(\rho) = (8+8\cos(\tfrac{2\pi}{M}))^{1/4} - 1 = 2\cos^{1/2}(\tfrac{\pi}{M}) - 1. \tag{85}$$

The previous results strongly suggest that, in general, for any q and for any p coprime with it, the only possible real value for $\cos(\rho)$, $|\cos(\rho)| \leq 1$, is

$$\cos(\rho) = \begin{cases} 2\cos^{2/q}(\frac{\pi}{M}) - 1, & \text{if } q \text{ is odd,} \\ 2\cos^{4/q}(\frac{\pi}{M}) - 1, & \text{if } q \text{ is even;} \end{cases} \tag{86}$$

remark that if q is odd, the angle ρ between two adjacent sides is the same for q and for $2q$. Although giving a universal proof that (86) holds for any q goes beyond the scope of this paper, we have checked it for a few more q. Moreover, it is absolutely in agreement with our numerical simulations, as we will see in Section 5. Therefore, we assume it is valid $\forall q$.

Once we have found the correct choice of ρ, we get immediately the value for $\hat{\psi}(0, t_{pq})$. Indeed, bearing in mind (59),

$$\hat{\psi}(0, t_{pq}) = \begin{cases} \frac{M\sqrt{q}}{2\pi} \arccos\left(2\cos^{2/q}(\frac{\pi}{M}) - 1\right), & \text{if } q \text{ is odd.} \\ \frac{M\sqrt{\frac{q}{2}}}{2\pi} \arccos\left(2\cos^{4/q}(\frac{\pi}{M}) - 1\right), & \text{if } q \text{ is even.} \end{cases} \tag{87}$$

It is straightforward to check that $\psi(0, t_{1,2}) = 1$. It is also interesting to note that

$$\begin{aligned} \lim_{q\to\infty} \hat{\psi}(0, t_{pq}) &= \frac{M\sqrt{2}}{\pi}(-\ln(\cos(\tfrac{\pi}{M})))^{1/2}, \\ \lim_{M\to\infty} \hat{\psi}(0, t_{pq}) &= 1. \end{aligned} \tag{88}$$

Moreover, $\mathbf{T}$, $\mathbf{e}_1$ and $\mathbf{e}_2$ can be completely determined for any p and q, too, up to a rigid movement. The same is valid for $\mathbf{X}$, obtained from integrating $\mathbf{T}$ once. In general, for an arbitrary polygon, it can be pretty complicated to specify the correct rigid movement. However, since our initial data is a regular planar polygon, the symmetries of the solution are very advantageous.

The easiest way to understand and to implement numerically the correct rotation (although not necessarily the simplest option for symbolic manipulation) is to work on $\mathbf{X}$, which depends only on $\mathbf{T}$. To that aim, given a time t_{pq}, we compute first the associated rotation matrices $\mathbf{M}_m$. Then, by means of (61), we obtain up to a rotation the piecewise constant vectors $\mathbf{T}$, $\mathbf{e}_1$ and $\mathbf{e}_2$, which we denote $\tilde{\mathbf{T}}$, $\tilde{\mathbf{e}}_1$ and $\tilde{\mathbf{e}}_2$:

$$\begin{pmatrix} \tilde{\mathbf{T}}(\frac{2\pi k}{Mq}^-)^T \\ \hline \tilde{\mathbf{e}}_1(\frac{2\pi k}{Mq}^-)^T \\ \hline \tilde{\mathbf{e}}_2(\frac{2\pi k}{Mq}^-)^T \end{pmatrix} = \begin{pmatrix} \tilde{\mathbf{T}}(\frac{2\pi k - 2\pi}{Mq}^+)^T \\ \hline \tilde{\mathbf{e}}_1(\frac{2\pi k - 2\pi}{Mq}^+)^T \\ \hline \tilde{\mathbf{e}}_2(\frac{2\pi k - 2\pi}{Mq}^+)^T \end{pmatrix}, \tag{89}$$

and the case $k = 0$ can be assigned any value, for instance the identity matrix, $(\tilde{\mathbf{T}}(0^-)|\tilde{\mathbf{e}}_1(0^-)|\tilde{\mathbf{e}}_2(0^-))^T = \mathbf{I}$. Let us underline that it is not necessary at all to consider separately q odd and q even. Indeed, in the case of q even, (63) and (65) safely allow us to regard the $Mq/2$-sided polygon as a *degenerated* Mq-sided polygon. This is extremely useful for implementation purposes.

Once $\tilde{\mathbf{T}}$ has been obtained, $\tilde{\mathbf{X}}$, which is $\mathbf{X}$ up to a rotation, is computed recursively:

$$\tilde{\mathbf{X}}(\tfrac{2\pi k+2\pi}{Mq}) = \tilde{\mathbf{X}}(\tfrac{2\pi k}{Mq}) + \tfrac{2\pi}{Mq}\tilde{\mathbf{T}}(\tfrac{2\pi k}{Mq}^+), \tag{90}$$

where, again, $\tilde{\mathbf{X}}(0)$ can be given any value, for instance $\tilde{\mathbf{X}}(0) = (0,0,0)^T$. To obtain the correct rotation for $\mathbf{X}$, we use the symmetries of the polygon, as explained in Section 3. In particular, we use the facts that, for any time t, $\mathbf{X}(2\pi k/M)$, $k = 0, \ldots, M-1$, have to be coplanar and lay on a plane orthogonal to the z-axis; and that $\mathbf{X}(2\pi/M) - \mathbf{X}(0)$ is a positive multiple of $(1,0,0)^T$. This can be done efficiently as follows:

1. Compute $\mathbf{v}^+ = \frac{\tilde{\mathbf{X}}(2\pi/M)-\tilde{\mathbf{X}}(0)}{\|\tilde{\mathbf{X}}(2\pi/M)-\tilde{\mathbf{X}}(0)\|}$, $\mathbf{v}^- = \frac{\tilde{\mathbf{X}}(0)-\tilde{\mathbf{X}}(-2\pi/M)}{\|\tilde{\mathbf{X}}(0)-\tilde{\mathbf{X}}(-2\pi/M)\|}$.
2. Compute $\mathbf{w} = \mathbf{v}^- \wedge \mathbf{v}^+$.
3. Compute the scalar product between $\mathbf{w}$ and $(0,0,1)^T$, $\mathbf{w} \cdot (0,0,1)^T = w_3$.
4. If $w_3 = 0$, $\mathbf{R}_1$ is the identity matrix. If not, $\mathbf{R}_1$ is the rotation matrix that induces a rotation of $\arccos(w_3)$ degrees around the axis given by the vector $\frac{\mathbf{w}\wedge(0,0,1)^T}{\|\mathbf{w}\wedge(0,0,1)^T\|}$.
5. Compute $\mathbf{v}^+_{new} = \mathbf{R}_1 \cdot \mathbf{v}^+$.
6. Compute the rotation matrix $\mathbf{R}_2$ that induces a rotation of $\arccos(\mathbf{v}^+_{new} \cdot (1,0,0)^T)$ degrees around the z-axis.
7. Compute the sought rotation matrix, $\mathbf{R} = \mathbf{R}_2 \cdot \mathbf{R}_1$.
8. Update $\mathbf{T} = \mathbf{R} \cdot \tilde{\mathbf{T}}$ and $\mathbf{X} = \mathbf{R} \cdot \tilde{\mathbf{X}}$.

By means of the previous algorithm, we have computed the correctly rotated values of $\mathbf{X}$ and $\mathbf{T}$. Additionally, for $\mathbf{X}$, we still have to specify a translation. Again, bearing in mind the symmetries of the problem, we translate $\mathbf{X}$ in such a way that its mass center, given by the mean of $\mathbf{X}(2\pi k/M)$, $k = 0, \ldots, M-1$, is in the z-axis. In this way, we have completely specified the position of $\mathbf{X}$, up to a vertical translation.

4. Numerical method

In this section, we simulate numerically (3) and (4) taking respectively (28) and (29) as initial data, i.e., $\mathbf{X}(s,0)$ is a planar regular polygon of M sides and length 2π.

There have been a couple of papers devoted to reproducing numerically the self-similar solutions of the Schrödinger map (4). In [8], a Crank-Nicholson scheme was consider, together with a finite-difference discretization of $\mathbf{T}_{ss}$. Later on, in [9], both finite-difference discretizations and pseudo-spectral discretizations were considered to simulate (4) and its equivalent on the hyperbolic plane. In particular, given the asymptotical structure of the self-similar solutions of (4), a truncated domain $s \in [-L, L]$, $L \gg 1$, with a grid based on the Chebyshev nodes was found to be very convenient to represent those solutions. Nevertheless, due to the clustering of the Chebyshev nodes, an explicit scheme to advance in time implied the undesirable restriction $|\Delta t| = \mathcal{O}(1/N^4)$, where N is the number of nodes. In order to solve that, it was chosen to work with the stereographic projection of $\mathbf{T} = (T_1, T_2, T_3)$ over $\mathbb{C}$,

$$z = x + iy \equiv (x, y) \equiv \left(\frac{T_1}{1+T_3}, \frac{T_2}{1+T_3}\right), \tag{91}$$

which transforms (4) into a nonlinear Schrödinger equation:

$$z_t = iz_{ss} - \frac{2i\bar{z}}{1+|z|^2} z_s^2. \tag{92}$$

The advantage of this equation, as opposed to (4), is that the higher-order term z_{ss} can be treated implicitly, therefore eliminating or at least reducing significantly the restrictions on Δt.

Working with (92) was a very adequate choice for the purposes of [9]. There, a second-order semi-implicit backward differentiation formula was chosen. This scheme was very stable because it imposed a very strong decay in the high frequency modes; moreover, its low order was easily and effectively compensated by the use of an adaptive method, both in space and in time.

However, in this paper, working with (92) does not seem to be such a good option. Indeed, unlike in [9], where an extremely high accuracy was required only for $0 < t \ll 1$, we are now interested in the behaviour of $\mathbf{T}$ **at all times**, for which a second-order scheme seems a very poor option.

After many unsuccessful attempts, which have greatly delayed the redaction of this paper, we admit that we have been unable to find a good higher-order scheme for (92). Furthermore, we are also interested in the evolution of $\mathbf{X}$, for which working with (92) is of limited help. Bearing in mind the previous arguments, we have opted to work directly with (4) or, more precisely, with a combination of (3) and (4):

$$\begin{cases}\mathbf{X}_t = \mathbf{T}\wedge\mathbf{T}_s,\\ \mathbf{T}_t = \mathbf{T}\wedge\mathbf{T}_{ss}.\end{cases} \tag{93}$$

In order to simulate numerically (93), we have chosen a fourth-order Runge-Kutta scheme in time:

$$\begin{aligned}
\mathbf{A}_X &= \mathbf{T}^{(n)}\wedge\mathbf{T}_s^{(n)}, \quad \mathbf{A}_T = \mathbf{T}^{(n)}\wedge\mathbf{T}_{ss}^{(n)}, \quad \mathbf{T}^{(A)} = \mathbf{T}^{(n)} + \tfrac{\Delta t}{2}\mathbf{A}_T,\\
\mathbf{B}_X &= \mathbf{T}^{(A)}\wedge\mathbf{T}_s^{(A)}, \quad \mathbf{B}_T = \mathbf{T}^{(A)}\wedge\mathbf{T}_{ss}^{(A)}, \quad \mathbf{T}^{(B)} = \mathbf{T}^{(n)} + \tfrac{\Delta t}{2}\mathbf{B}_T,\\
\mathbf{C}_X &= \mathbf{T}^{(B)}\wedge\mathbf{T}_s^{(B)}, \quad \mathbf{C}_T = \mathbf{T}^{(B)}\wedge\mathbf{T}_{ss}^{(B)}, \quad \mathbf{T}^{(C)} = \mathbf{T}^{(n)} + \Delta t\mathbf{C}_T,\\
\mathbf{D}_X &= \mathbf{T}^{(C)}\wedge\mathbf{T}_s^{(C)}, \quad \mathbf{D}_T = \mathbf{T}^{(C)}\wedge\mathbf{T}_{ss}^{(C)},\\
\mathbf{X}^{(n+1)} &= \mathbf{X}^{(n)} + \tfrac{\Delta t}{6}(\mathbf{A}_X + 2\mathbf{B}_X + 2\mathbf{C}_X + \mathbf{D}_X),\\
\tilde{\mathbf{T}} &= \mathbf{T}^{(n)} + \tfrac{\Delta t}{6}(\mathbf{A}_T + 2\mathbf{B}_T + 2\mathbf{C}_T + \mathbf{D}_T), \quad \mathbf{T}^{(n+1)} = \frac{\tilde{\mathbf{T}}}{\|\tilde{\mathbf{T}}\|}.
\end{aligned} \tag{94}$$

The last line guarantees that $\mathbf{T}^{(n)}\in\mathbb{S}^2$, $\forall n$. Additionally, we can also project $\mathbf{T}^{(A)}$, $\mathbf{T}^{(B)}$, $\mathbf{T}^{(C)}$ onto the unit sphere, but we have noticed no significant improvement in our numerical results.

We have combined the previous Runge-Kutta scheme with a pseudo-spectral discretization directly in space. More precisely, since we deal with periodic solutions in $s\in[0,2\pi)$, we have simulated the evolution of $\mathbf{X} = (X_1, X_2, X_3)$ and $\mathbf{T} = (T_1, T_2, T_3)$ at N equally spaced nodes $s_j = 2\pi j/N$, $j = 0,\dots,N-1$. In order to compute $\mathbf{T}_s$, $\mathbf{T}_{ss}$, etc., we remember that, given a periodical function $f(s)$ evaluated at s_j, its derivatives at s_j can be spectrally approximated as

$$f_s(s_j) = \sum_{k=-N/2}^{N/2-1} ik\hat{f}(k)e^{2\pi ijk/N}, \quad f_{ss}(s_j) = -\sum_{k=-N/2}^{N/2-1} k^2\hat{f}(k)e^{2\pi ijk/N}, \tag{95}$$

where

$$\hat{f}(k) = \sum_{j=0}^{N-1} f(s_j)e^{-2\pi ijk/N}. \tag{96}$$

Both (95) and (96), wich are respectively inverse and direct discrete Fourier transforms (DFT), can be computed efficiently by means of the Fast Fourier Transform (FFT) algorithm [24]. Moreover, since $\mathbf{X}$ and $\mathbf{T}$ are invariant by rotations of $2\pi/M$ degrees around the z-axis, as shown in (32), we can reduce the computational cost of (95) and (96) to a DFT of N/M elements, instead of a DFT of N elements. In what follows, we explain how to apply this idea to $\mathbf{T}$. This is valid, with no change, for any vector satisfying (32), i.e., $\mathbf{X}$, $\mathbf{T}_s$, $\mathbf{T}_{ss}$, etc. First, let us consider the first two components of $\mathbf{T}$. Denoting $Z(s_j) = T_1(s_j,t) + iT_2(s_j,t)$, we have

$$\begin{aligned}
\hat{Z}(k) &= \sum_{j=0}^{N-1} Z(s_j)e^{-2\pi ijk/N} \\
&= \sum_{l=0}^{M-1}\sum_{j=0}^{N/M-1} Z(s_{j+l(N/M)})e^{-2\pi i(j+l(N/M))k/N} \\
&= \left(\sum_{l=0}^{M-1} e^{-2\pi il(k-1)/M}\right)\sum_{j=0}^{N/M-1} Z(s_j)e^{-2\pi ijk/N} \\
&= \begin{cases} M\displaystyle\sum_{j=0}^{N/M-1} Z(s_j)e^{-2\pi ijk/N}, & \text{if } k \equiv 1 \mod M, \\ 0, & \text{if } k \not\equiv 1 \mod M. \end{cases}
\end{aligned} \tag{97}$$

Therefore, the only non-zero $Z(k)$ are those with $k \equiv 1 \mod M$. Moreover, they can be obtained by a DFT of N/M elements instead of a DFT of N elements:

$$\begin{aligned}
\hat{Z}(Mk+1) &= M\sum_{j=0}^{N/M-1} Z(s_j)e^{-2\pi ij(Mk+1)/N} \\
&= M\sum_{j=0}^{N/M-1}\left[e^{-2\pi ij/N}Z(s_j)\right]e^{-2\pi ijk/(N/M)}.
\end{aligned} \tag{98}$$

Identically for the third component of $\mathbf{T}$,

$$\begin{aligned}
\hat{T}_3(k) &= \sum_{j=0}^{N-1} T_3(s_j)e^{-2\pi ijk/N}\\
&= \sum_{l=0}^{M-1}\sum_{j=0}^{N/M-1} T_3(s_{j+l(N/M)})e^{-2\pi i(j+l(N/M))k/N}\\
&= \left(\sum_{l=0}^{M-1} e^{-2\pi ilk/M}\right)\sum_{j=0}^{N/M-1} T_3(s_j)e^{-2\pi ijk/N}\\
&= \begin{cases} M\displaystyle\sum_{j=0}^{N/M-1} T_3(s_j)e^{-2\pi ijk/N}, & \text{if } k\equiv 0 \mod M,\\ 0, & \text{if } k\not\equiv 0 \mod M. \end{cases}
\end{aligned} \tag{99}$$

Therefore, the only non-zero $\hat{T}_3(k)$ are those with $k \equiv 0 \mod M$ and, again, they can be obtained by a DFT of N/M elements instead of a DFT of N elements:

$$\hat{T}_3(Mk) = M\sum_{j=0}^{N/M-1} T_3(s_j)e^{-2\pi ijk/(N/M)}. \tag{100}$$

Furthermore, since $T_3(s)$ is real, this last expression can be further simplified to a DFT of $N/(2M)$ elements.

Combining (94) with a pseudo-spectral discretization in space, we obtain a scheme with a time-step restriction on Δt that appears to be of the form $\Delta t \le C/N^2$, with $C \approx 11.3$. However, for a fixed M, we only want to simulate $\mathbf{X}$ and $\mathbf{T}$ for $t \in [0, 2\pi/M^2]$. Denoting Δt_{max} the biggest Δt that makes (94) stable, the smallest number of time-steps N_t needed to reach $t = 2\pi/M^2$ is of at least

$$N_t \ge \left\lceil \frac{2\pi/M^2}{\Delta t_{max}} \right\rceil = \left\lceil \frac{2\pi/M^2}{C/N^2} \right\rceil = \left(\frac{N}{M}\right)^2 \left\lceil \frac{2\pi}{C} \right\rceil. \tag{101}$$

From this equation, together with (98) and (100), it follows that, for a given $r \in \mathbb{N}$, if we take $N = 2^r M$, i.e., the computational cost for simulating (94) is exactly the same for any number of initial sides M, no matter how big it is. This important fact enables us to make consistent comparisons between different M, because we are considering an equivalent spatial resolution, i.e, we are simulating the same number of points N/M. We take N/M a power of two to take the greatest possible advantage of the FFT. Obviously, for N/M constant, Δt decreases as $\mathcal{O}(1/M^2)$; therefore, the most accurate results will be expected for the largest M, as we will see in our numerical experiments.

In the following section, we simulate $\mathbf{X}$ and $\mathbf{T}$ for initial data with different M. As we will see, despite its simplicity, (94) gives surprisingly good results.

5. Numerical experiments

In Section 3, in order to construct algebraically the evolution of a regular polygon at rational times, we have done some very strong assumptions, the most important one being uniqueness. However, as we will see in this section, the numerical experiments are in complete agreement with their theoretical predictions. To illustrate this, we have simulated the evolution of $\mathbf{X}$ and $\mathbf{T}$ by means of (94), taking regular polygons with different numbers of sides M as initial data, and making $\mathbf{X}$ and $\mathbf{T}$ evolve until $t = 2\pi/M^2$. The initial data $\mathbf{X}(s, 0)$ and $\mathbf{T}(s, 0)$ are given respectively by (28) and (29); obviously, in the case of $\mathbf{X}$, the non-vertex points are immediately computed by linear interpolation. We have taken N equally-spaced nodes $s_j = 2\pi j/N \in [0, 2\pi)$, $0, \ldots, N-1$; nevertheless, bearing in mind the symmetries of $\mathbf{X}$ and $\mathbf{T}$ as described in the previous section, we only have to describe the evolution of $\mathbf{X}$ and $\mathbf{T}$ at the first N/M nodes $s_j \in [0, 2\pi/M)$, $j = 0, \ldots, N/M - 1$. We have divided the time-interval $[0, 2\pi/M^2]$ in N_t equally-spaced time steps of length $\Delta t = \frac{2\pi}{M^2 N_t}$. Therefore, during the simulation of (94), we obtain $\mathbf{X}^{(n)}$ and $\mathbf{T}^{(n)}$, at $t^{(n)} = n\Delta t$, $n = 1, \ldots, N_t$. In our experiments, bearing in mind (101), we have chosen $N_t = 151200 \cdot 4^r$, for $N/M = 512 \cdot 2^r$.

Remember that, in Section 3, we had constructed algebraically $\mathbf{X}$ up to a vertical movement. Therefore, in order to completely specify $\mathbf{X}$ at a given time, we would need to give the height of one point or, more conveniently, the height $h(t)$ of the mass center, which is precisely the mean of all the values $X_3(s_j, t)$:

$$h(t) = \frac{1}{N}\sum_{j=0}^{N-1} X_3(s_j, t) = \frac{M}{N}\sum_{j=0}^{N/M-1} X_3(s_j, t). \tag{102}$$

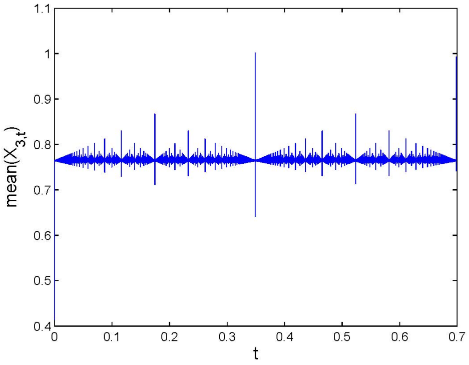

Figure 2: Evolution of $h'(t) = \text{mean}(X_{3,t})$ against t, for an initial triangle, $M = 3$, $N = 3 \times 4096$ nodes.

On the one hand, $h'(t)$, computed numerically by

$$\begin{aligned} h'(t) &= \frac{1}{N}\sum_{j=0}^{N-1} X_{3,t}(s_j, t) \\ &= \frac{1}{N}\sum_{j=0}^{N-1}(X_{1,s}(s_j,t)X_{2,ss}(s_j,t) - X_{2,s}(s_j,t)X_{1,ss}(s_j,t)), \end{aligned} \tag{103}$$

is far from constant and has a very singular shape, as shown in Figure 2, where we have plotted the numerical evolution of $h'(t)$, at all $t^{(n)} = n\Delta t$, for an initial triangle, $M = 3$, $N = 3 \times 4096$ nodes.

On the other hand, when integrating $h'(t)$, the oscillations cancel and completely disappear. Furthermore, $h(t)$ can be approximated with great accuracy by means of a constant multiplied by t; more precisely,

$$h(t) \approx \frac{h(2\pi/M^2)}{2\pi/M^2} t = c_M t, \tag{104}$$

where $c_M = h(\frac{2\pi}{M^2})/\frac{2\pi}{M^2}$ is the mean speed. In Table 1, we give the maximum discrepancy between $h(t)$ and its linear approximation $c_M t$, i.e., $\max_n |h(t^{(n)}) - c_M t^{(n)}|$. We have considered different M and different numbers of nodes N; the errors are very small and they seem to decrease as $\mathcal{O}(1/N)$. This gives very strong evidence that $h(t)$ is linear or, at least, quasi-linear. Therefore, in practice, we can safely assume that $h(t) = c_M t$. Observe that c_M, which

M	$N/M = 512$	$N/M = 1024$	$N/M = 2048$	$N/M = 4096$	c_M
3	$4.3096 \cdot 10^{-5}$	$2.1206 \cdot 10^{-5}$	$1.0886 \cdot 10^{-5}$	$5.7953 \cdot 10^{-6}$	0.7645
4	$1.2398 \cdot 10^{-6}$	$6.1344 \cdot 10^{-6}$	$3.2140 \cdot 10^{-6}$	$1.7316 \cdot 10^{-6}$	0.8827
5	$4.8504 \cdot 10^{-6}$	$2.4191 \cdot 10^{-6}$	$1.2807 \cdot 10^{-6}$	$6.9338 \cdot 10^{-7}$	0.9286
6	$2.2848 \cdot 10^{-6}$	$1.1441 \cdot 10^{-6}$	$6.0905 \cdot 10^{-7}$	$3.3044 \cdot 10^{-7}$	0.9517
7	$1.2167 \cdot 10^{-6}$	$6.1060 \cdot 10^{-7}$	$3.2607 \cdot 10^{-7}$	$1.7710 \cdot 10^{-7}$	0.9651
8	$7.0721 \cdot 10^{-7}$	$3.5594 \cdot 10^{-7}$	$1.9014 \cdot 10^{-7}$	$1.0333 \cdot 10^{-7}$	0.9735
9	$4.3905 \cdot 10^{-7}$	$2.2140 \cdot 10^{-7}$	$1.1828 \cdot 10^{-7}$	$6.4303 \cdot 10^{-8}$	0.9792
10	$2.8697 \cdot 10^{-7}$	$1.4489 \cdot 10^{-7}$	$7.7407 \cdot 10^{-8}$	$4.2093 \cdot 10^{-8}$	0.9832

Table 1: $\max_n |h(t^{(n)}) - c_M t^{(n)}|$, for different numbers of initial sides M, and of nodes N. $t^{(n)} = n\Delta t$; $c_M = h(\frac{2\pi}{M^2})/\frac{2\pi}{M^2}$. The values corresponding to c_M have been calculated with $N/M = 4096$.

is also offered in Table 1 for $N/M = 4096$, grows with M, tending to 1, as M tends to infinity, i.e. as $\mathbf{X}(s,0)$ tends to a circle.

In order to compare the values of $\mathbf{X}$ obtained numerically, which we label $\mathbf{X}_{num}$, with those obtained algebraically, which we label $\mathbf{X}_{alg}$, we have subtracted the vertical position of the center of mass from $\mathbf{X}_{num}$, i.e., we have analyzed the agreement between $\mathbf{X}_{num} - c_M t(0,0,1)^T$ and $\mathbf{X}_{alg}$. More precisely, we have computed $\max_m(\max_j \|\mathbf{X}_{num}(s_j, t^{(m)}) - c_M t^{(m)}(0,0,1)^T - \mathbf{X}_{alg}(s_j, t^{(m)})\|)$, where $s_j = 2\pi j/N$, $j = 0, \cdots, N/M - 1$; $\|\cdot\|$ denotes the Euclidean distance; and $t^{(m)} = \frac{2\pi}{M^2} \cdot \frac{m}{1260}$, $m = 0, \ldots, 1260$. Notice that, in Section 3, we have constructed $\mathbf{X}_{alg}(s,t)$ only at the vertices, so the non-vertex points $\mathbf{X}_{alg}(s_j, t)$ are computed again by linear interpolation. Observe also that comparing $\mathbf{X}_{num}$ and $\mathbf{X}_{alg}$ at $N_t + 1$ time-instants would have been computationally unrealistic. Instead, we have chosen $1260 + 1$ time-instants, because 1260 is a number large enough for our purposes, and with a convenient factorization, $1260 = 2^2 \cdot 3^2 \cdot 5 \cdot 7$.

The maximum value of $\|\mathbf{X}_{num}(s_j, t^{(m)}) - c_M t^{(m)}(0,0,1)^T - \mathbf{X}_{alg}(s_j, t^{(m)})\|$ is given in Table 2, for different N/M and M. Bearing in mind that we are comparing $\mathbf{X}_{num}$ and $\mathbf{X}_{alg}$ globally for a large number of nodes and time-instants, and that $\max \|\mathbf{X}_{alg}\| > 1$, $\forall M$, the results are, in our opinion, very remarkable, and strongly suggest that there is convergence, or at least an extremely good agreement, between both approaches, as $N \to \infty$; moreover, since $\mathbf{X}_{alg}$ is periodical in time, with time-period $2\pi/M^2$, they also suggest that $\mathbf{X}$ is periodical, or at least quasi-periodical, in time with that period, up to a vertical movement. All this is also supported by the fact that the

M	$N/M = 512$	$N/M = 1024$	$N/M = 2048$	$N/M = 4096$
3	$2.4847 \cdot 10^{-3}$	$1.3841 \cdot 10^{-3}$	$8.1211 \cdot 10^{-4}$	$4.9718 \cdot 10^{-4}$
4	$1.1221 \cdot 10^{-3}$	$6.9665 \cdot 10^{-4}$	$4.2717 \cdot 10^{-4}$	$2.5917 \cdot 10^{-4}$
5	$6.8414 \cdot 10^{-4}$	$4.2545 \cdot 10^{-4}$	$2.6125 \cdot 10^{-4}$	$1.5874 \cdot 10^{-4}$
6	$4.6057 \cdot 10^{-4}$	$2.8717 \cdot 10^{-4}$	$1.7670 \cdot 10^{-4}$	$1.0754 \cdot 10^{-4}$
7	$3.3170 \cdot 10^{-4}$	$2.0724 \cdot 10^{-4}$	$1.2772 \cdot 10^{-4}$	$7.7832 \cdot 10^{-5}$
8	$2.5059 \cdot 10^{-4}$	$1.5680 \cdot 10^{-4}$	$9.6744 \cdot 10^{-5}$	$5.9010 \cdot 10^{-5}$
9	$1.9616 \cdot 10^{-4}$	$1.2288 \cdot 10^{-4}$	$7.5878 \cdot 10^{-5}$	$4.6313 \cdot 10^{-5}$
10	$1.5782 \cdot 10^{-4}$	$9.8943 \cdot 10^{-5}$	$6.1137 \cdot 10^{-5}$	$3.7334 \cdot 10^{-5}$

Table 2: $\max_m(\max_j \|\mathbf{X}_{num}(s_j, t^{(m)}) - c_M t^{(m)}(0,0,1)^T - \mathbf{X}_{alg}(s_j, t^{(m)})\|)$, where $s_j = \frac{2\pi j}{N}$, $j = 0, \cdots, N/M - 1$; $\|\cdot\|$ denotes the Euclidean distance; and $t^{(m)} = \frac{2\pi}{M^2} \cdot \frac{m}{1260}$, $m = 0, \ldots, 1260$.

errors decreases as M increases. Indeed, from (101), we are taking the same number of time-steps N_t for each M, but $\Delta t = \frac{2\pi}{M^2 N_t}$, i.e., $\Delta t = \mathcal{O}(1/M^2)$, which explains those smaller values for the last rows of Table 2 and also of Table 1.

On the other hand, comparing the algebraically constructed $\mathbf{T}_{alg}$ with the numerically obtained $\mathbf{T}_{num}$ is more problematic. For example, in Figure 3, we have compared $\mathbf{T}_{num}$ (left) with $\mathbf{T}_{alg}$ (right), for an initial triangle, $M = 3$, at $t_{1,3} = \frac{2\pi}{27}$, $N/M = 4096$. The exact value of $\mathbf{T}$ at that time is given by $\mathbf{T}_{alg}$, which, by construction, is a piecewise constant function with exactly $qM = 9$ pieces, that we denote $\mathbf{T}_i$, $i = 1, \ldots, 9$, and whose explicit values, in this case, have an easy algebraic expression:

$$\mathbf{T}_1 = \begin{pmatrix} \sqrt[3]{2} - 1 \\ -\sqrt{\sqrt[3]{4} - 1} \\ 1 - \sqrt[3]{4} \end{pmatrix}, \quad \mathbf{T}_2 = \begin{pmatrix} 1 \\ 0 \\ 0 \end{pmatrix}, \quad \mathbf{T}_3 = \begin{pmatrix} \sqrt[3]{2} - 1 \\ \sqrt{\sqrt[3]{4} - 1} \\ \sqrt[3]{4} - 1 \end{pmatrix}; \tag{105}$$

$\mathbf{T}_4$, $\mathbf{T}_5$ and $\mathbf{T}_6$ are respectively $\mathbf{T}_1$, $\mathbf{T}_2$ and $\mathbf{T}_3$ rotated $\frac{2\pi}{3}$ degrees around the z-axis; $\mathbf{T}_7$, $\mathbf{T}_8$ and $\mathbf{T}_9$ are respectively $\mathbf{T}_1$, $\mathbf{T}_2$ and $\mathbf{T}_3$ rotated $\frac{4\pi}{3}$ degrees around the z-axis. Observe that $\mathbf{T}_{num}$ is almost identical to $\mathbf{T}_{alg}$, but clearly exhibits a Gibbs-type phenomenon. However, in $\mathbf{T}_{num}$, if we take the central values of each interval (altogether 27 circles, indicated in Figure 2 with a black circle), and compare them componentwise with (105), we obtain a maximum error equal to $6.3869 \cdot 10^{-9}$.

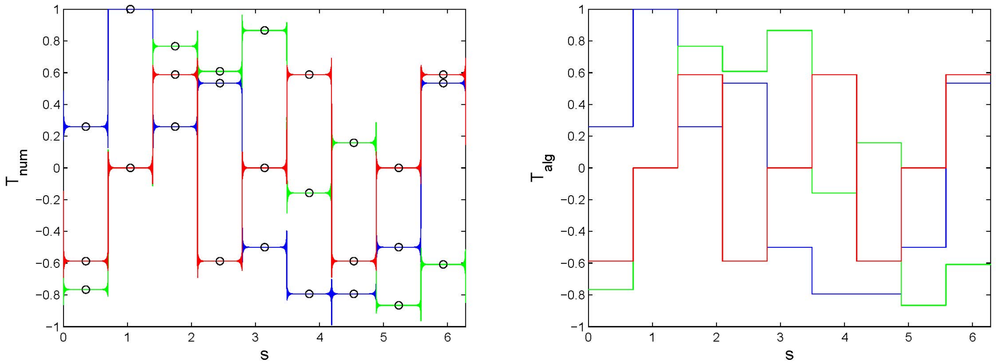

Figure 3: $\mathbf{T}_{num}$ versus $\mathbf{T}_{alg}$, for $M = 3$, at $t_{1,3} = \frac{2\pi}{27}$. T_1 appears in blue, T_2 in green, T_3 in red. In $\mathbf{T}_{num}$, the Gibbs phenomenon is clearly visible. The black circles denote the points chosen for the comparisons.

5.1. $\mathbf{X}(0,t)$ *and Riemann's non-differentiable function*

Bearing in mind the mirror symmetries of the initial data, as illustrated for the pentagon in Figure 1, we conclude that $\mathbf{X}(\pi k/M, t)$, $k = 0, \ldots, 2M-1$, lives in a plane that contains the z-axis. Indeed, $s = \pi k/M$ are the only points such that $\mathbf{X}(s,t)$ describe a planar curve. In what follows, we will describe $\mathbf{X}(0,t)$, although all said here is immediately applicable to any $s = \pi k/M$. Since $\mathbf{X}(0,t) = (X_1(0,t), X_2(0,t), X_3(0,t))$ is planar, bearing in mind that $X_1(0,t) < 0$, $X_2(0,t) < 0$, we rotate $\mathbf{X}(0,t)$ clockwise $\pi/2 - \pi/M$ degrees around the z-axis, until it lays on the plane OYZ, which we identify with $\mathbb{C}$. Then $\mathbf{X}(0,t)$ becomes

$$z(t) = -\|(X_1(0,t), X_2(0,t))\| + iX_3(0,t). \tag{106}$$

In Figure 4, we have plotted the numerically obtained $z(t)$ for different M. Besides the conspicuous fractal character of the curves, which immediately reminds us of the works [10, 11], their most striking feature (see Figure 5) is how much $z(t) - ic_M t$, i.e., z(t) without the vertical movement, resembles the graph of

$$\phi(t) = \sum_{k=1}^{\infty} \frac{e^{\pi i k^2 t}}{i\pi k^2}, \quad t \in [0,2]. \tag{107}$$

$\phi(t)$ was conveniently used in [17], in order to study Riemann's non-differen-

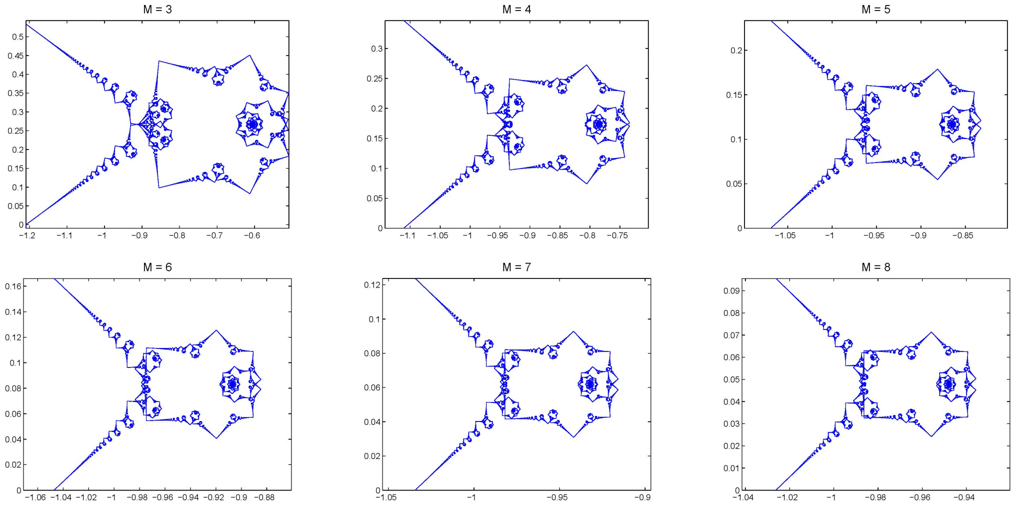

Figure 4: $z(t)$, for $M = 3, 4, 5, 6, 7, 8$. $N/M = 4096$. We have plotted the $z(t)$ corresponding to all the $N_t + 1$ points $\mathbf{X}^{(n)}(0)$ obtained during the execution of (94).

tiable function, which is precisely the real part of $\phi(t)$, i.e.,

$$f(t) = \sum_{k=1}^{\infty} \frac{\sin(\pi k^2 t)}{\pi k^2}. \tag{108}$$

$f(t)$ is non-differentiable everywhere, except at those rational points $t = p/q$, with p and q both odd. On the other hand, when constructing algebraically $\mathbf{X}(0, t)$ for a given t, we have observed that the only times at which $\mathbf{X}(0, t)$ has no corner are of the form $t_{pq} = \frac{2\pi p}{M^2 q}$, with p odd and $q \equiv 2 \mod 4$. Therefore, in order to compare $\phi(t)$ and $\mathbf{X}(0, t)$, we have to redefine slightly $\phi(t)$ in (107):

$$\phi(t) = \frac{\pi}{6} - \sum_{k=1}^{\infty} \frac{e^{2\pi i k^2 t}}{\pi k^2}, \quad t \in [0, 1], \tag{109}$$

i.e., we multiply ϕ in (107) by $-i$, in order to orientate it correctly; then we translate it, so $\phi(0) = \phi(1) = 0$, and, finally, we change its period from $t \in [0, 2]$ to $t \in [0, 1]$.

On the other hand, given M, we compare ϕ in (109) with

$$z_M(t) \equiv z(\tfrac{2\pi t}{M^2}) - z(0) - i c_M \tfrac{2\pi t}{M^2}, \quad t \in [0, 1]. \tag{110}$$

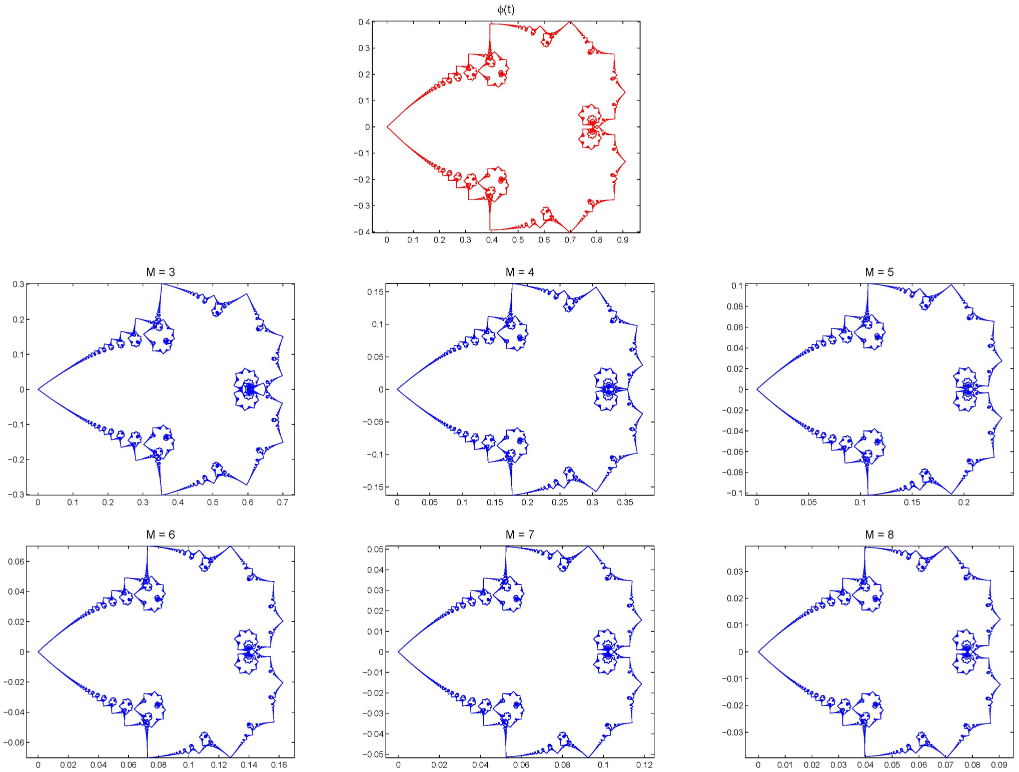

Figure 5: $\phi(t)$ (red), as defined in (109), against $z_M(t)$ (blue), for $M = 3, 4, 5, 6, 7, 8$. To compute $\phi(t)$, we took $\sum_{k=0}^{4096-1}$. To compute, $z_M(t)$, we took $N/M = 4096$. We have plotted the $z_M(t)$ corresponding to all the $N_t + 1$ points $\mathbf{X}^{(n)}(0)$ obtained during the execution of (94).

In Figure 5, we have plotted $\phi(t)$ (red), as defined in (109), versus $z_M(t)$, for different M. Although the figures are not identical, they are extremely similar. Moreover, if we scale them accordingly, it seems that the bigger M grows, the more similar to $\phi(t)$ is $z_M(t)$. In what follows, we will give some evidence that this indeed happens.

Since we have obtained numerically $z_M(t)$ at $N_t + 1$ points $t \in [0, 1]$, we have to evaluate $\phi(t)$ precisely at those points. Then, we scale $z_M(t)$, approximating the scale factor in this way:

$$\lambda_M = \frac{\max\limits_{t\in[0,1]} Re(\phi(t))}{\max\limits_{t\in[0,1]} Re(z_M(t))}.$$

M	$\|\phi(t) - \lambda_M z_M(t)\|_{L^\infty}$
3	$9.2128 \cdot 10^{-2}$
4	$4.7210 \cdot 10^{-2}$
5	$2.9124 \cdot 10^{-2}$
6	$1.9899 \cdot 10^{-2}$
7	$1.4517 \cdot 10^{-2}$
8	$1.1091 \cdot 10^{-2}$
9	$8.7713 \cdot 10^{-3}$
10	$7.1269 \cdot 10^{-3}$

Table 3: Maximum error between $\phi(t)$ and $z_M(t)$ (scaled). To compute $\phi(t)$, we took $\sum_{k=0}^{4096-1}$. To compute $z_M(t)$, we took $N/M = 4096$. We have considered the $z_M(t)$ corresponding to all the $N_t + 1$ points $\mathbf{X}^{(n)}(0)$ obtained during the execution of (94). We have computed algebraically $\phi(t)$ at those times.

Finally, we compute $\|\phi(t) - \lambda_M z_M(t)\|_{L^\infty}$. Table 3 shows the errors obtained in this way for several M. Bearing in mind that $\max_{t\in[0,1]} |\phi(t)| \approx 0.9187$, that the scaling λ_M was not intended to be optimal, and that we are comparing $9676800 + 1$ different points one by one, the results give a pretty strong evidence of that convergence. This gives strong support to the idea that z_M is also a multifractal, $\forall M \geq 3$.

As we mentioned in the introduction, the proof that $f(t)$ is a multifractal was done in [18]. In this respect, it is fundamental the identity given for ϕ, as defined in (107), which states that

$$\phi(t) = \phi(t_{pq}) + e^{\pi i m/4} q^{-1/2} (t - t_{pq})^{1/2} + \text{ lower-order terms}, \tag{111}$$

with $p, q \in \mathbb{Z}$, $q > 0$, $\gcd(p, q) = 1$, $m \equiv m(t_{pq}) \in \mathbb{Z}/8\mathbb{Z}$. This identity is proved in Theorem 4.2 in [17]. Of particular relevance is the fact that the Hölder exponent is $1/2$, i.e., that $|\phi(t) - \phi(t_{pq})| = q^{-1/2}|t - t_{pq}|^{1/2} +$ lower-order terms.

In order to prove analytically that $z_M(t)$, is a multifractal, we would need an equivalent of (111). We have made some numerical experiments (see for example Figure 6, for $M = 3$, $p = 1$, $q = 5$), and all of them give strong evidence that the Hölder exponent of $z(t)$ is $1/2$ for rational times, i.e., that $|z_M(t) - z_M(t_{pq})| = \mathcal{O}(|t - t_{pq}|^{1/2})$.

Nevertheless, how the constants depend of the denominator q, something which is a fundamental ingredient in the arguments in [17] and in [18], is

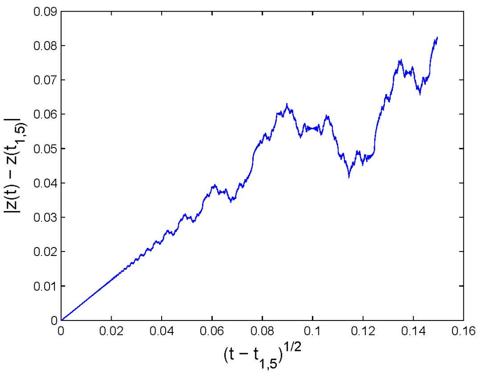

Figure 6: $|z(t) - z(t_{1,5})|$ versus $(t - t_{1,5})^{1/2}$, for $M = 3$. The asymptotically linear relation between both quantities as $t \to t_{1,5}$ is evident.

unclear. This question deserves a much more detailed analysis that we plan to make in a forthcoming paper.

5.2. $\mathbf{T}(s, t_{pq})$*, for* $q \gg 1$

In the previous subsection, we have given evidence of the multifractal character of $\mathbf{X}(0, t)$. However, in [9], fractal-like phenomena were observed also on $\mathbf{T}$, when imposing periodic boundary conditions. In the following lines, we will show that similar observations are valid for periodic boundary conditions, too.

As we have seen in this paper, $\mathbf{X}$ can be recovered algebraically up to a vertical movement, while $\mathbf{T}$ can be completely recovered algebraically at rational times. Furthermore, $\mathbf{T}_{alg}$ is really a piecewise constant function, with no noise associated to the Gibbs phenomenon. This gives us a very powerful tool to progress in the understanding of $\mathbf{T}$ (and also of $\mathbf{X}$), avoiding numerical simulations at all.

A very interesting question is, given a rational time $t_{pq} = \frac{2\pi p}{M^2 q}$, with q *small*, corresponding in $\mathbf{X}$ to a polygon of Mq or $Mq/2$ sides, and in $\mathbf{T}$ to a piecewise continuous function with Mq or $Mq/2$ jumps, what happens at a time $t + \varepsilon$, $|\varepsilon| \ll 1$?

Let us take $\varepsilon = \frac{2\pi}{M^2 q'}$, with $q' \gg 1$, in order that $|\varepsilon| \ll 1$. Assuming that $\gcd(q, q') = 1$, then, $\frac{p}{q} + \frac{1}{q'} = \frac{pq'+1}{qq'}$, so $t + \varepsilon$ would correspond to a polygon of qq' or $qq'/2$ sides.

In Figure 7, we have have plotted $\mathbf{X}_{alg}$ and $\mathbf{T}_{alg}$, for $M = 3$, at $t = \frac{2\pi}{9}(\frac{1}{4}+$

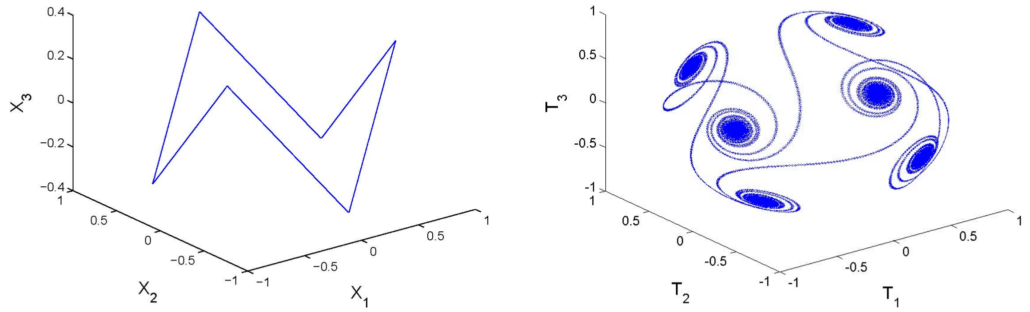

Figure 7: $\mathbf{X}_{alg}$ and $\mathbf{T}_{alg}$, at $t = \frac{2\pi}{9}(\frac{1}{4} + \frac{1}{49999})$.

$\frac{1}{49999}) = \frac{2\pi}{9} \cdot \frac{50003}{199996}$. While visually there is no difference whatsoever between $\mathbf{X}_{alg}$ at $t_{1,4} = \frac{2\pi}{9} \cdot \frac{1}{4}$ and $\mathbf{X}_{alg}$ at $t = \frac{2\pi}{9} \cdot \frac{50003}{199996}$, we do not have a skew polygon with 6 sides, but a skew polygon with $Mq/2 = 299994$ sides that closely resembles a polygon with 6 sides. On the other hand, the corresponding $\mathbf{T}_{alg}$ are very different. Indeed, in the plot of $\mathbf{T}_{alg}$, we can clearly appreciate six spiral-like structures whose centers are precisely the six constant values of $\mathbf{T}$ at $t_{1,4}$. Nevertheless, it is important to underline that these structures are not really spirals, but the plot of the 299994 different values taking by $\mathbf{T}$, that closely resembles a curve with six spirals. Furthermore, these spirals remind us of the Cornu spirals that appeared in [6]. An open question that arises naturally is up to what extent the multiple-corner problem can be explained as a sum of several one-corner problems.

Another interesting question is what happens if we take a time t_{pq} with *large* q, such that there is no pair (p', q'), with both q' and $|\frac{p}{q} - \frac{p'}{q'}|$ *small*. In this case, the situation is very different. In Figure 8, we have plotted $\mathbf{X}_{alg}$ and $\mathbf{T}_{alg}$ for $M = 3$, at $t = \frac{2\pi}{9}(\frac{1}{4} + \frac{1}{41} + \frac{1}{401}) = \frac{2\pi}{9} \cdot \frac{18209}{65764}$. While the left-hand side is not so different from the left-hand side of Figure 7, the right-hand side is a set of $Mq/2 = 98646$ points in $\mathbb{S}^2$ that creates a spectacular fractality sensation with spiral-like structures at three or four different scales. This can be better appreciated in Figure 9, where we have plotted the stereographic projection of $\mathbf{T}$ onto $\mathbb{C}$.

In general, a time t_{pq}, with $q \gg 1$, can be regarded as an approximation of an irrational time. Trying to fully understand the phenomena exhibited by $\mathbf{T}(s, t)$ at those times is a challenging question that we postpone for the

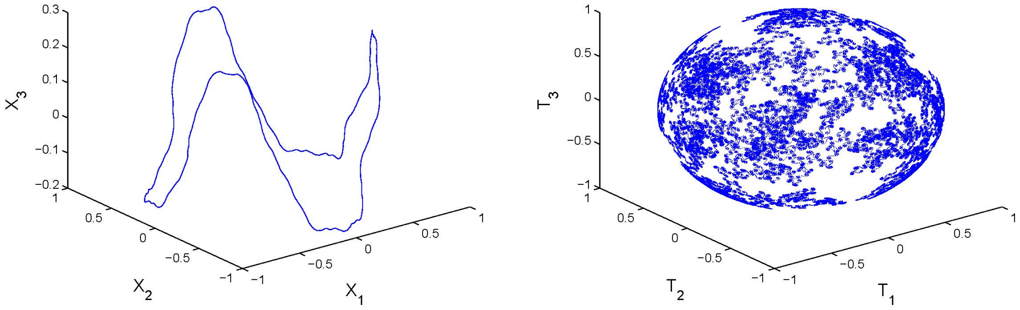

Figure 8: $\mathbf{X}_{alg}$ and $\mathbf{T}_{alg}$, at $t = \frac{2\pi}{9}(\frac{1}{4} + \frac{1}{41} + \frac{1}{401}) = \frac{2\pi}{9} \cdot \frac{18209}{65764}$.

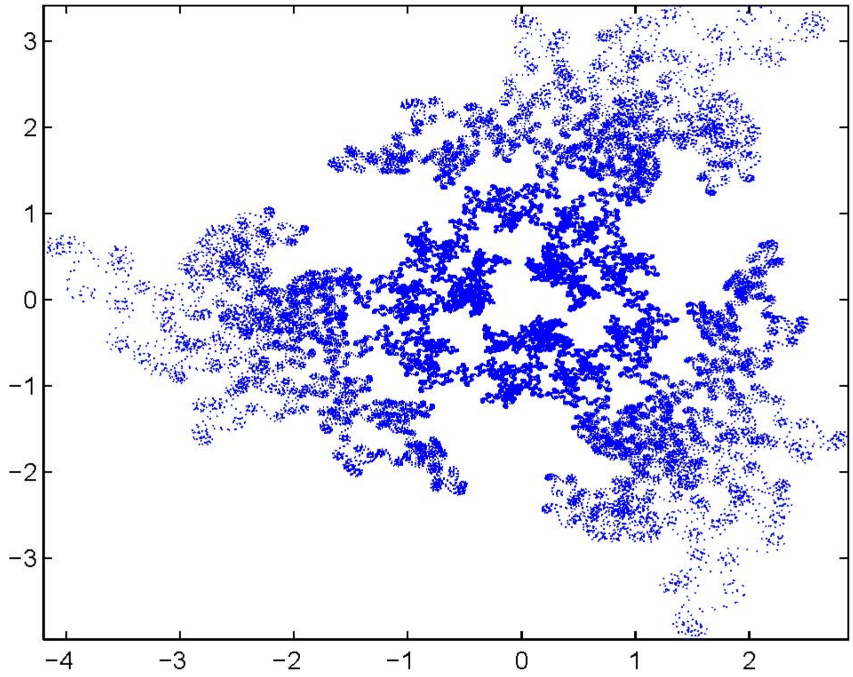

Figure 9: Stereographic projection of the right-hand side of Figure 8.

future.

6. Conclusions

In this paper, we have studied the evolution of (3) and (4), for a regular planar polygonal of M sides as initial datum. The algebraic calculations, backed by complete numerical simulations, suggest very strongly that $\mathbf{X}(s,t)$ is a polygon at times which are rational multiples of $2\pi/M^2$, i.e., $t_{pq} = (2\pi/M^2)(p/q)$, with the number of sides depending on q, while $\mathbf{T}(s,t)$ is piecewise constant at those times.

We have obtained a striking connection between $\mathbf{X}(0,t)$ and the so-called Riemann's non-differentiable function. In [18], S. Jaffard proved that this function is an example of multifractal whose spectrum of singularities satisfies the Frisch-Parisi conjecture. Although there is strong numerical evidence that $\mathbf{X}(0,t)$ is also a multifractal, an analytical proof seems to be challenging. In fact, a first step in this direction is giving sense to our solutions from an analytical point of view. Moreover, while our $\mathbf{X}(s,t)$, obtained algebraically for rational times, can be extended by continuity to all $t \in \mathbb{R}$, it is not clear how to give sense to $\mathbf{T}(s,t)$ at irrational times.

In the future, we also plan to extend these ideas to arbitrary polygons, and to do a more detailed study on fractality. For such purposes, a more complete algebraically description of $\mathbf{X}$ and $\mathbf{T}$ is no doubt required. More precisely, we would aim at a level of detail similar to that in (86).

Acknowledgements

The authors wish to thank V. Banica and F. Chamizo for enlightening conversations. This work was supported by MEC (Spain), with the project MTM2011-24054.

Appendix A. Generalized Quadratic Gauß Sums

The generalized quadratic Gauß sums are defined by

$$G(a,b,c) = \sum_{l=0}^{|c|-1} e^{2\pi i(al^2+bl)/c}, \tag{A.1}$$

for given integers a, b, c, with $c \neq 0$. From now on, we assume $c > 0$, and $\gcd(a,c) = 1$, which are the cases dealt with in this paper.

The value of these sums was calculated for the first time by Gauß for the case $b = 0$ [25]. More precisely, given two integers a, c such that $\gcd(a, c) = 1$, then

$$G(a,0,c) = \sum_{l=0}^{c-1} e^{2\pi i a l^2/c} = \begin{cases} (\frac{c}{a})(1+i^a)\sqrt{c}, & \text{if } c \equiv 0 \mod 4, \\ (\frac{a}{c})\sqrt{c}, & \text{if } c \equiv 1 \mod 4, \\ 0, & \text{if } c \equiv 2 \mod 4, \\ (\frac{a}{c})i\sqrt{c}, & \text{if } c \equiv 3 \mod 4, \end{cases} \tag{A.2}$$

where $(\frac{a}{c})$ denotes the Jacobi symbol.

As we will see in the following lines, the generalized quadratic Gauß sums can be reduced to normal quadratic Gauß sums by completing the square. Since they are multiplicative, i.e.,

$$G(a,b,cd) = G(ac,b,d)G(ad,b,c), \quad \text{with } \gcd(c,d) = 1, \tag{A.3}$$

we can assume without loss of generality that c is either odd or a power of two. If c is odd, let us find a certain $\psi(a)$ such that $4a\psi(a) \equiv 1 \mod c$. This $\psi(a)$ is unique modulo c and is precisely the inverse of $4a$ in $\mathbb{Z}/c\mathbb{Z}$; since $\gcd(4a, c) = 1$, its existence is guaranteed by Bézout's lemma, and it can be efficiently computed, for instance, by the extended Euclidean algorithm. Then, we have

$$\begin{aligned} G(a,b,c) &= \sum_{l=0}^{c-1} e^{2\pi i(al^2+4a\psi(a)bl+\psi(a)b^2-\psi(a)b^2)/c} \\ &= e^{-2\pi i\psi(a)b^2/c} \sum_{l=0}^{c-1} e^{2\pi i(al^2+4a\psi(a)bl+4a\psi(a)\psi(a)b^2)/c} \\ &= e^{-2\pi i\psi(a)b^2/c} \sum_{l=0}^{c-1} e^{2\pi i a(l+2\psi(a)b)^2/c} \\ &= e^{-2\pi i\psi(a)b^2/c} \sum_{l=0}^{c-1} e^{2\pi i a l^2/c} \\ &= \begin{cases} e^{-2\pi i\psi(a)b^2/c}(\frac{a}{c})\sqrt{c}, & \text{if } c \equiv 1 \mod 4, \\ e^{-2\pi i\psi(a)b^2/c}(\frac{a}{c})i\sqrt{c}, & \text{if } c \equiv 3 \mod 4. \end{cases} \end{aligned} \tag{A.4}$$

If c is a power of two, we first observe that

$$\begin{aligned} G(a,b,c) &= \sum_{l=0}^{c/2-1} e^{2\pi i(al^2+bl)/c} + \sum_{l=0}^{c/2-1} e^{2\pi i(a(l+c/2)^2+b(l+c/2))/c} \\ &= \left[1+(-1)^{a(c/2)+b}\right] \sum_{l=0}^{c/2-1} e^{2\pi i(al^2+bl)/c} \\ &= \begin{cases} 0, & \text{if } a(c/2) \not\equiv b \mod 2, \\ 2\sum_{l=0}^{c/2-1} e^{2\pi i(al^2+bl)/c}, & \text{if } a(c/2) \equiv b \mod 2; \end{cases} \end{aligned}$$

therefore, we have two cases: $c = 2$ and $c > 2$. If $c = 2$, then a is odd, so

$$G(a,b,2) = \begin{cases} 0, & \text{if } b \text{ is even,} \\ 2, & \text{if } b \text{ is odd.} \end{cases} \tag{A.5}$$

On the other hand, if $c > 2$, $G(a,b,c) = 0$, if b is odd. Let us suppose b is even. Then, since a is odd, we follow the previous reasoning to find a certain $\psi(a)$ such that $a\psi(a) \equiv 1 \mod c$, so

$$\begin{aligned} G(a,b,c) &= \sum_{l=0}^{c-1} e^{2\pi i(al^2+a\psi(a)2(b/2)l+\psi(a)(b/2)^2-\psi(a)(b/2)^2)/c} \\ &= e^{-\pi i\psi(a)b^2/(2c)} \sum_{l=0}^{c-1} e^{2\pi i(al^2+2a\psi(a)(b/2)l+a\psi(a)\psi(a)(b/2)^2)/c} \\ &= e^{-\pi i\psi(a)b^2/(2c)} \sum_{l=0}^{c-1} e^{2\pi ia(l+\psi(a)(b/2))^2/c} \\ &= e^{-\pi i\psi(a)b^2/(2c)} \sum_{l=0}^{c-1} e^{2\pi ial^2/c} \\ &= e^{-\pi i\psi(a)b^2/(2c)} (\tfrac{c}{a})(1+i^a)\sqrt{c}. \end{aligned} \tag{A.6}$$

In general, given an arbitrary $c \in \mathbb{N}$, we will factorize it as $c = 2^r c'$ and use the multiplicative character of the generalized quadratic Gaussian sums to calculate $G(a,b,c)$. For instance, if c is even, but $c/2$ is odd, then

$$\begin{aligned} G(a,b,c) &= G(a,b,2(c/2)) \\ &= G(a(c/2),b,2)G(2a,b,c/2) \\ &= \begin{cases} 0, & \text{if } a(c/2) \not\equiv b \mod 2, \\ 2G(2a,b,c/2), & \text{if } a(c/2) \equiv b \mod 2, \end{cases} \end{aligned} \tag{A.7}$$

i.e, $G(a,b,c) = 0$, if b is even, etc.

To conclude this appendix, we will mention the explicit value of $|G(a,b,c)|$, deduced from the previous calculations, which is of especial relevance in this paper. If $\gcd(a,c) = 1$, then

$$|G(a,b,c)| = \begin{cases} \sqrt{c}, & \text{if } c \text{ is odd}, \\ \sqrt{2c}, & \text{if } c \text{ is even and } c/2 \equiv b \mod 2, \\ 0, & \text{if } c \text{ is even and } c/2 \not\equiv b \mod 2. \end{cases} \tag{A.8}$$

References

References

[1] L. S. Da Rios. On the motion of an unbounded fluid with a vortex filament of any shape. *Rend. Circ. Mat. Palermo*, 22:117–135, 1906. In Italian.

[2] R. J. Arms and F. R. Hama. Localized-Induction Concept on a Curved Vortex and Motion of an Elliptic Vortex Ring. *Phys. Fluids*, 8(4):553–559, 1965.

[3] G. K. Batchelor. *An Introduction to Fluid Dynamics*. Cambridge Mathematical Library. Cambridge University Press, 1967.

[4] P. G. Saffman. *Vortex Dynamics*. Cambridge Monographs on Mechanics. Cambridge University Press, 1995.

[5] L. D. Landau and E. M. Lifshitz. On the theory of the dispersion of magnetic permeability in ferromagnetic bodies. *Phys. Z. Sowjet.*, 8(2):153–169, 1935.

[6] S. Gutiérrez, J. Rivas, and L. Vega. Formation of singularities and self-similar vortex motion under the localized induction approximation. *Comm. PDE*, 28(5–6):927–968, 2003.

[7] F. de la Hoz. Self-similar solutions for the 1-D Schrödinger map on the hyperbolic plane. *Math. Z.*, 257(1):61–80, 2007.

[8] T. F. Buttke. A Numerical Study of Superfluid Turbulence in the Self-Induction Approximation. *J. Comput. Phys.*, 76(2):301–326, 1998.

[9] F. de la Hoz, C. J. García-Cervera, and L. Vega. A Numerical Study of the Self-Similar Solutions of the Schrödinger Map. *SIAM J. Appl. Math.*, 70(4):1047–1077, 2009.

[10] C. S. Peskin and D. M. McQueen. Mechanical equilibrium determines the fractal fiber architecture of the aortic heart valve leaflets. *Am. J. Physiol.*, 266(1):H319–H328, 1994.

[11] J. V. Stern and C. S. Peskin. Fractal dimension of an aortic heart valve leaflet. *Fractals*, 2(3):461–464, 1994.

[12] R. L. Jerrard and D. Smets. On the motion of a curve by its binormal curvature. 2011. arXiv:1109.5483 [math.DG].

[13] C. E. Kenig, G. Ponce, and L. Vega. On the ill-posedness of some canonical dispersive equations. *Duke Math. J.*, 106(3):617–633, 2001.

[14] Valeria Banica and Luis Vega. Scattering for 1D cubic NLS and singular vortex dynamics. *J. Eur. Math. Soc. (JEMS)*, 14(1):209–253, 2012.

[15] Valeria Banica and Luis Vega. Stability of the selfsimilar dynamics of a vortex filament. 2012. arXiv:1202.1106 [math.AP].

[16] Valeria Banica and Luis Vega. The initial value problem for the Binormal Flow with rough data. 2013. preprint.

[17] J. J. Duistermaat. Selfsimilarity of “Riemann’s Nondifferentiable function”. *Nieuw Arch. Wisk.*, (4) 9(3):303–337, 1991.

[18] S. Jaffard. The spectrum of singularities of Riemann’s function. *Rev. Mat. Iberoamericana*, 12(2):441–460, 1996.

[19] U. Frisch and G. Parisi. *Fully developped turbulence and intermittency.* Proc. Int. Sch. Phys. "Enrico Fermi", North-Holland, Amsterdam, 1985.

[20] U. Frisch. *Turbulence. The Legacy of A. N. Kolmogorov.* Cambridge University Press, 1995.

[21] L. Kapitanski and I. Rodnianski. Does a Quantum Particle Know the Time? *Emerging Applications of Number Theory, IMA Vol. Math. Appl.*, 109:355–371, 1999.

[22] H. Hasimoto. A soliton on a vortex filament. *J. Fluid Mech.*, 51(3):477–485, 1972.

[23] G. Trenkler and D. Trenkler. On the product of rotations. *Int. J. Math. Educ. Sci. Tech.*, 39(1):94–104, 2008.

[24] M. Frigo and S. G. Johnson. The design and implementation of FFTW3. *Proc. IEEE*, 93(2):216–231, 2005.

[25] B. C. Berndt, R. J. Evans, and K. S. Williams. *Gauss and Jacobi Sums.* Canadian Mathematical Society Series of Monographs and Advanced Texts. John Wiley and Sons, Inc., 1998.